Geometric High-Frequency Models and Potential Analogs for the Determination of Current and Field Distributions

A. Knobloch, J. Mantel, G. Roos,
H. Schlageter, F. Werner

IPP 4/30 Mai 1966

INSTITUT FÜR PLASMAPHYSIK

GARCHING BEI MÜNCHEN

INSTITUT FÜR PLASMAPHYSIK

GARCHING BEI MÜNCHEN

Geometric High-Frequency Models and Potential Analogs for the Determination of Current and Field Distributions

A. Knobloch, J. Mantel, G. Roos,
H. Schlageter, F. Werner

IPP 4/30 Mai 1966

The contents of this report will be presented at the 4th Symposium on Engineering Problems in Thermonuclear Research, Frascati - Rome 23 - 27 May 1966

Die nachstehende Arbeit wurde im Rahmen des Vertrages zwischen dem Institut für Plasmaphysik GmbH und der Europäischen Atomgemeinschaft über die Zusammenarbeit auf dem Gebiete der Plasmaphysik durchgeführt.

IPP 4/30

Geometric High-Frequency Models and Potential Analogs for the Determination of Current and Field Distributions

A. Knobloch, J. Mantel, G. Roos, H. Schlageter, F. Werner

Mai 1966

1. Abstract

For the choice of electrical and other data for fast capacitor banks used for experiments in plasma physics the project engineer useds observations and measurements made on appropriate models. The following report describes the models of various collector and load configurations and discusses the measurements made on them.

I n d e x

1. Abstract

2. Introduction

3. Account of the experiments

3.1 Plane models of plate-type collector configurations

3.1.1 Object of the measurements

3.1.2 Determining the inductance of plate-type devices, the current density distribution and the electromagnetic forces from the field of flow

3.1.2.1 Conditions

3.1.2.2 The plane steady field of flow

3.1.2.3 Graphical method of determining the field of flow of plate-type conductor devices

3.1.2.4 Sheet manganin models

3.1.2.5 Determining the inductance of the configuration from the field of flow

3.1.2.6 Determining the electromagnetic forces from the field of flow

3.1.3 Model, feeding, measuring device

3.1.3.1 Accuracy of the results

3.2 Model of collector + coil of the 1,5/2,6 MJ bank

3.2.1 Object of the measurements

3.2.2 The problem

3.2.3 Model

3.2.4 Results

3.2.4.1 Direction of current

3.2.4.2 Current density distribution

3.3 HF-fed models

3.3.1 Frequency

3.3.2 Feeding

3.3.3 Measurement device

3.3.3.1 Coil-probes

3.3.3.2 Measurement accuracy

3.3.4 Copper model of the collector and the coil of the 1,5/2,6 MJ bank Isar I

3.3.4.1 Aim of the measurement

3.3.4.2 Models

3.3.4.3 Feeding

3.3.4.4 Measurement results

3.3.5 Model of the collector extension in the 1,5/2,6 MJ bank Isar I

3.3.5.1 Aim of the measurement

3.3.5.2 Model, feeding

3.3.5.3 Measurement results

3.3.6 Model of the double fed coil of the 10 kJ Turbulence Heating Experiment

3.3.6.1 Double fed coil

3.3.6.2 Problems

3.3.6.3 Model

3.4 Spatial and surface potential distribution problems simulated in the electrolytic tank

3.4.1 A model of the "Isar I" collector made of insulating material

3.4.2 The servo plotter system

3.4.3 Electronic equipment

3.4.3.1 Probe head and inpedance transformer

3.4.3.2 Angular position system

3.4.3.3 Linear shifting system

3.4.3.4 Power supply

3.4.3.5 Appendix to 3.4.3.1

3.5 Tests on components and on detail models of invidual parts and critical sections

3.5.1 Current tests

3.5.1.1 Contacts for the 1,5/2,6 MJ capacitor bank

3.5.1.2 144 kJ test bank

3.5.1.3 Plug contacts

3.5.1.4 Low-current models

3.5.2 Voltage tests

3.6 Electrical analogon to the collector motion

3.6.1 Model of the collector of the 1,5/2,6 MJ capacitor bank Isar I

3.6.1.1 Measurements

2. Introduction

Before a start is made to planning the main data of the new experimental set-up are chosen, namely current programme, coil dimensions, flux density. The first task of the project engineer is now to select the elements of the discharge circuit which will give the required discharge data, i.e. to determine the necessary capacitance, permissible inductance and damping of the discharge circuit.

Since it links up the discharge cable and load (coil) the collector is one element whose inductance may be affected to a very great extent by the design. The influence of the geometrical dimensions on the inductance of plate-type collector configurations was therefore investigated in appropriate models. Once the individual elements have been roughly determined so as to provide the necessary discharge data the electrical and mechanical stress on the individual components has to be evaluated.

The dimensions of parts subject to severe electrical stress (edges, the overlap area of foils) are investigated in detail models.

Furthermore of importance are a knowledge of cooperative effects, a firm grasp of earthing problems and information on the quality of the magnetic field in the coil (i.e. knowledge of the homogeneity and symmetry of the magnetic field).

With respect to the last three points spatial models were prepared and analogue measurements in an electrolytic tank were made.

3. Account of the experiments

3. 1. Plane models of plate-type collector configurations

3. 1.1 Object of the measurements

The measurements were made as a basis for determining the technical data of plate-type collector configurations. These data are

a) Inductance
b) Current density at the coil connection
c) Distribution of forces over the plates and centre of gravity of the forces.

3. 1.2 Determining the inductance of plate-type devices, the current density distribution and the electromagnetic forces from the field of flow.

3. 1.2.1 Conditions

The following conditions are valid for nearly all collector configurations:

1) The discharge of the bank takes the form of a damped oscillation with a frequency of 25 kHz ./. 400 kHz or a crowbar pulse.

2) The plate separation is small relative to the other dimensions and is equal all over the plate region.

3) The penetration depth of the current is small compared with the thickness of the conducting layer.

4) Then the original flow is approximately a potential flow.

3. 1.2.2 The plane steady field of flow

The field of flow described above can be reproduced in model form by a steady field of flow. Two scales are introduced:

1) The mechanical scale according to which the geometrical dimensions are converted.

2) The electrical scale according to which the value of the flowing current is converted.

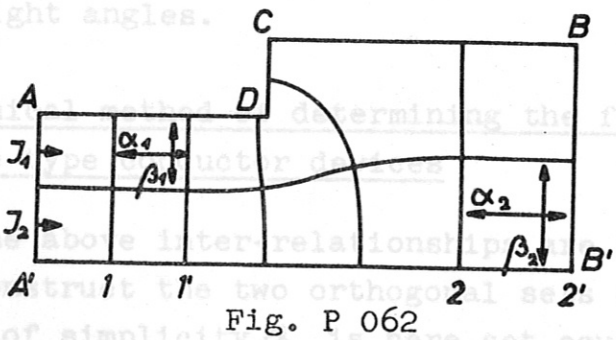

Fig. P 062

Fig. P 062 shows a field of flow. The current is applied via the line AA', leaving the region under investigation at the line BB'. The locus of a streaming particle reproduces a streamline and two streamlines define a stream duct. The lines ADCB and A'B' are thus streamlines as well. If the region traversed is divided up into several stream ducts of equal branch current the field of flow gives an illustrative

picture of the current density distribution in the region investigated. The current density at each point of the field of flow is given by: the branch current divided by (width of the stream duct normal to the direction of the current times the thickness of the conducting medium). The equipotential lines run orthogonally to the stream-lines. The potential difference between two adjacent equipotential lines should be constant:

$U_1 = J_1 \cdot R_1$ between the points 1 and 1'

$U_2 = J_2 \cdot R_2$ between the points 2 and 2'

$$U_1 = J_1 \cdot \varrho_1 \cdot \frac{\alpha_1}{d_1 \cdot \beta_1}$$

$$U_2 = J_2 \cdot \varrho_2 \cdot \frac{\alpha_2}{d_2 \cdot \beta_2}$$

d = thickness of the conducting medium.

In the case of uniformly conducting material we obtain

$\varrho_1 = \varrho_2$ and $d_1 = d_2$

It was postulated that $J_1 = J_2$ and $U_1 \doteq U_2$

and so $\frac{\alpha_1}{\beta_1} = \frac{\alpha_2}{\beta_2}$

Streamlines and equipotential lines thus form a network of geometrically similar meshes whose sides intersect at right angles.

3. 1.2.3 Graphical method of determining the field of flow of plate-type conductor devices

If the above inter-relationships are known it is possible to construct the two orthogonal sets of curves. For the sake of simplicity α is here set equal to β, i.e. a network consisting of square-like figures is produced. As a rule, a few interation processes give the correct field pattern.

3. 1.2.4 Sheet manganin models

Representing a field of flow in the form of a model calls for a conductive material. Suitable for plane models are graphite paper and sheet manganin.

In the geometrically simple field regions we are concerned with, sheet manganin is preferable to graphite paper because of its superior homogeneity and strength. The set of curves of the equipotential lines is measured, the feeding of the model being in correct proportion to the original.

The streamlines orthogonal to the equipotential lines can be constructed very quickly.

3. 1.2.5 Determining the inductance of the configuration from the field of flow

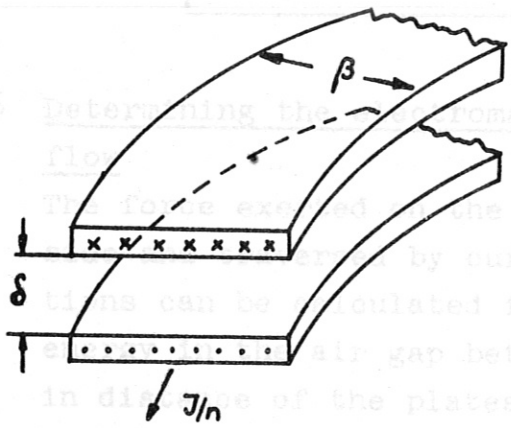

Fig. P 063

Fig. P 063 shows a single stream duct from fig. P 062, traversed by branch current I/n and showing the opposite plate. According to the conditions described in 3.1.2.1 a magnetic field strength exists - apart from the boundary regions - only in the air space between the two plates.

Consequently one has for the magnetic field strength

$$H = \frac{J}{n \cdot \beta}$$

and for the magnetic energy

$$Wm = \frac{1}{2} \mu o \cdot \mu r \cdot H^2 \cdot Vol$$

In the air space ($\mu r = 1$) between two square-like meshes:

$$W_m^{\square} = \frac{1}{2} \mu o \cdot \frac{J^2}{n^2 \cdot \beta^2} \cdot \delta \cdot \alpha \cdot \beta \; ; \quad \alpha = \beta$$

$$W_m^{\square} = \frac{1}{2} \mu o \cdot \frac{J^2}{n^2} \cdot \delta$$

The total magnetic energy of the plate-type conductor device is

$Wm = z \cdot W_{mm}^{\square}$; Z = total number of meshes

$$W_m = \frac{1}{2} z \cdot \mu_o \cdot \frac{J^2}{n^2} \cdot \delta$$

The self-inductance of a configuration is defined by the magnetic energy of the configuration according to the relation:

$$L = \frac{2 \cdot Wm}{J^2}$$

The inductance is thus $L = \mu_o \cdot \frac{Z}{n^2} \cdot \delta$

$$\boxed{\frac{L}{nH} = 4\pi \cdot \frac{Z}{n^2} \cdot \frac{\delta}{cm}}$$

3. 1.2.6 Determining the electromagnetic forces from the field of flow

The force exerted on the two plates positioned side by side and traversed by currents flowing in opposite directions can be calculated from the variation of the magnetic energy in the air gap between the two plates by the change in distance of the plates:

$$F = \frac{\partial Wm}{\partial \delta}$$

$$F = \frac{1}{2} \mu_o \cdot Z \cdot \frac{J^2}{n^2}$$

$$\boxed{\frac{F}{Kp} = \frac{10.2}{2} \cdot \mu_o \cdot \frac{1}{n^2} \cdot \frac{J^2}{A^2}}$$

Each mesh of the network of streamlines and equipotential lines constructed according to 3.1.2.2 is acted upon by the same force

$$\frac{F^{\square}}{Kp} = 5{,}1 \cdot 4\pi \cdot 10^{-9} \cdot \frac{1}{n^2} \cdot \frac{J^2}{A^2}$$

It is thus possible to state the pressure distribution on the plates by writing the mean pressure for the area

of a mesh:

$$\sigma = \frac{F^{\square}}{d_i^2}$$

di = width of the stream duct at the place under investigation.

For the total force in a parallel plate system, whose inductance is known, one has

$$\frac{F_{tot}}{Kp} = 5{,}1 \cdot 10^{-9} \cdot \frac{J^2}{A^2} \cdot \frac{L}{nH} \cdot \frac{cm}{\delta}$$

3. 1.3 Model, feeding, measuring device

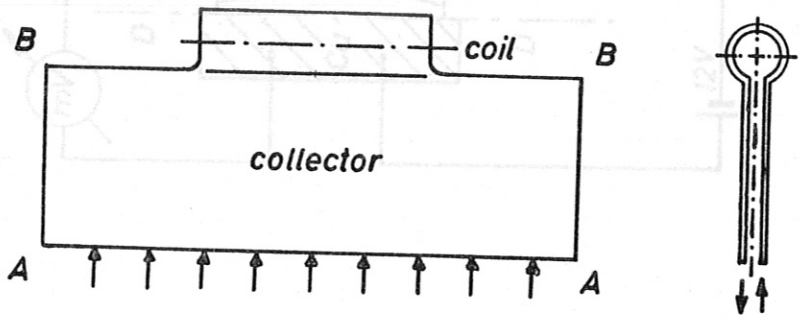

Fig. P 064 shows a collector configuration (conducting layer without steel pressure plates). The current is applied uniformly along the line $\overline{AA}$ via coaxial cables; the load which takes the form of a one-turn coil is connected to the contact line $\overline{BB}$.

The corresponding plane analogue model is shown in fig. P 065.

Equal input currents I/n are produced by connecting in series to each input terminal a resistance large relative to that of a stream duct.

The field of flow and the field of the equipotential lines are symmetric to the streamline $\overline{CC}$ and the equipotential line $\overline{DD}$ and they do not vary if the current is collected at a copper plate soldered on along $\overline{DD}$. The final model set-up is thus as follws: Fig. P 066

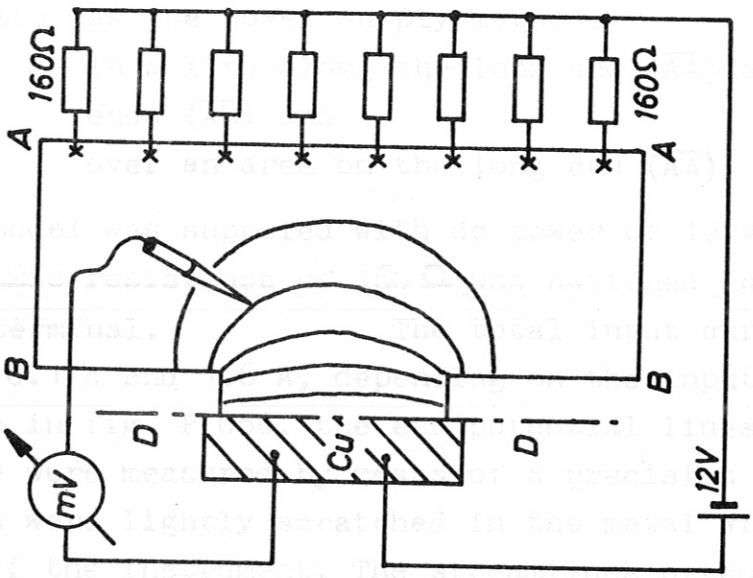

Fig. P 066

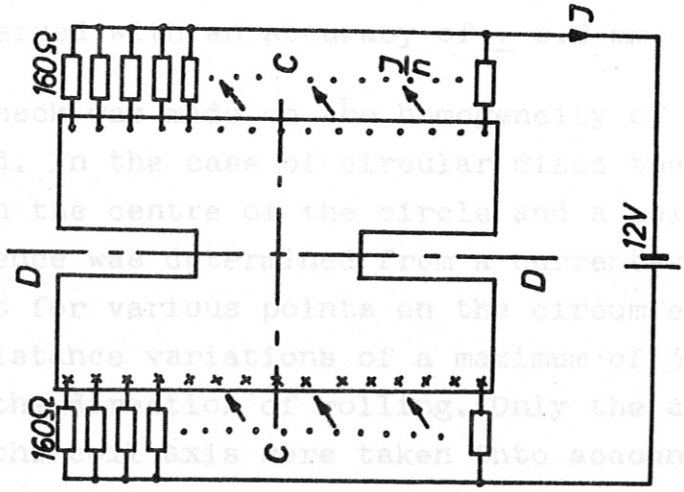

Fig. P 065

In the models described the following three geometrical dimensions were varied:

plate width
coil diameter
coil length

as also was the power supply method:

in a line along the long end ($\overline{AA}$) and the short ends ($\overline{AB}$) and
over an area on the long end ($\overline{AA}$)

The model was supplied with dc power of 12 V. An ohmic resistance of 160 Ω was switched in for each input terminal. The total input current was between 0.1 A and 1.6 A, depending on the input method. As shown in fig. P 066, the equipotential lines to the copper plate were measured by means of a precision instrument. The lines were lightly scratched in the metal with the testing tip of the instrument. The streamlines orthogonal to this set of curves were graphically determined and the inductance found by counting off the meshes. The current density distribution at the coil connection was measured as a quantity proportional to the voltage at a strip 5 mm wide (double probe).

3. 1.3.1 Accuracy of the results

Care should be taken to solder on the Cu plate properly right along the line of symmetry $\overline{DD}$. This condition was observed with an accuracy of ± o.2 mm.

A check was made on the homogeneity of the sheet manganin used. In the case of circular discs the resistance between the centre of the circle and a point on the circumference was determined from a current-voltage measurement for various points on the circumference. This gave resistance variations of a maximum of 3.7 %, irrespective of the direction of rolling. Only the components normal to the coil axis were taken into account in the current measurement.

No appreciable asymmetry occured in the field pattern. Only in a few models the measured path of the equipotential lines was in the outer region of the plates, where the lines are far apart, slightly different in the two halves. Since, however, the greater part of the magnetic energy is to be found in the air space below the centre part of the plates and the vicinity of the coil connection, the influence exerted on the inductance determined remains small. At worst, the difference of the inductances, these being determined in each case from the field pattern of the individual halves of the plates, from that determined from the two halves of the plates is 0.88 % and 1.17 % respectively. (See also IPP Report 4/6).

3.2 Model of collector and coil of the 1.5/2.6 MJ bank

3.2.1 Object of the measurements

To influence the direction at the current in the coil by making slots in the conducting layer.
Influence of slots on the current density distribution in the coil connection.

3.2.2 The problem

The magnetic field in the discharge coil is expected to give homogeneity right to the end of the coil if possible. However, the result of the geometrical dimensions chosen for the collector plates according to 3.1 is that at the contact line $\overline{BB}$ (fig. P 064) the current in the vicinity the coil ends has a component in the direction of the coil axis. Because of the close proximity of the coil to the edge $\overline{BB}$ of the collector the current in the coil also has an axial component at the ends of the coil. The orthogonal arrangement of the current and excited field produces a radial component of the field, the latter already becoming inhomogeneous within the coil.

Making appropriate slots in the conducting layer in front of the coil connection brings about a radial flow into the coil.

3. 2.3 Model

The conducting layer of the collector + coil configuration was represented with sheet manganin on a scale of 1 : 10. The discharge coil comprises 5 coil sections, The region immediately in front of the coil slot is divided up by 150 parallel slots measuring 50 mm x 1 mm in the original. This corresponds in the original to the area between the coil slot and the contacts being slotted, this being a favourable solution for design purposes.

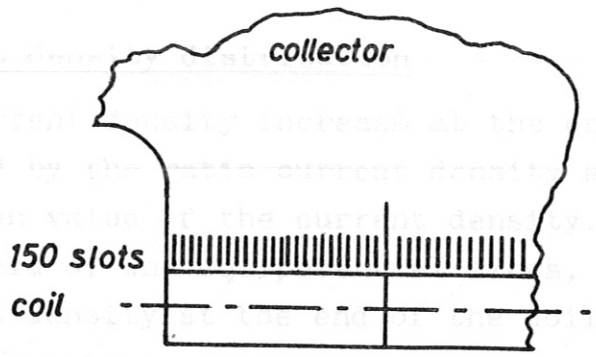

Fig. P 068

The model was supplied with direct current; an ohmic resistance of 160 Ω was switched in at each input terminal to ensure equal input currents.

The current density distribution over the length of the coil in the axial direction was determined in respect of size and direction as a voltage drop over 1/4 of the coil periphery.

3. 2.4 Results

The measurements were made each time with slotted and unslotted conducting layer.

With a dc power supply the measurements do not show the current density distributions and excessive current increases occurring in the original operation (with HF power the current density distribution becomes uniform). These measurements, however, are a quick and convenient way of checking the effectiveness of a particular operation, e.g. slotting the conducting layer. It is from this angle that

the model measurements described in 3. 2.1 should be understood.

3. 2.4.1 Direction of current

The fields of the equipotential lines were plotted before and after the slots were made. The influence exerted by the slots becomes obvious from the smaller curvature of the equipotential lines in the vicinity of the coil slot. Evaluation must be restricted to this merely qualitative statement.

3. 2.4.2 Current density distribution

The current density increase at the end of the coil is defined by the ratio current density at the coil end over the mean value of the current density. As can be seen from the field of the equipotential lines, the increase of the current density at the end of the coil in the slotted model is greater:

$$\frac{J_{max}}{J_{mean}} = 1.33 \quad \text{slotted}$$

$$= 1.28 \quad \text{unslotted}$$

The measurements made on the sheet manganin models were repeated on the copper models scaled 1:5 described in the following under 3. 3.4 by way of a check: The same shape of curve was obtained for the current density distribution and almost the same values for the increase of the current density.

3.3. HF-fed models

3.3.1 Frequency

In order to obtain a scaled model for current distribution problems, a corresponding model frequency has to be chosen considering the skin depth.

Following applies for the skin depth:

$$d_E = \sqrt{\frac{2}{w \cdot \varkappa \cdot \mu}}$$

$$\frac{d_E \text{ model}}{d_E \text{ original}} = \sqrt{\frac{w_0 \cdot \varkappa_0 \cdot \mu_0}{w_m \cdot \varkappa_m \cdot \mu_m}} = \frac{1}{M}$$

In most cases the model conductor is made of the original material; so the model frequency must be chosen M^2 times the original frequency.

There are also problems in which the wave length must be to scale or the model frequency should be M times of the original one: for shielding problems, design of earth lines a.s.o.

3. 3.2 Feeding

The model is fed by HF currents which are generated either by HF generators for steady state measurements or by pulse generators for transient measurements.

In the steady state case, the signal is amplified in a tuned amplifier or adjusted by a high quality air-core transformer.

For transient measurement pulses are used with regular wave forms from convertical pulse generators, or with practice shapes as actually appear by using of a switching analog system, which will be reported separately.+) For the pulse measurement a broad band amplifier with high current output must be used. This amplifier has been developed in the IPP and is under construction at the moment. It has the following data:

band width: 3 kHz - 800 kHz
output current: 40 amps.

The amplifier has two equal outputs, whereby it is possible to dephase the output currents head-on for some angular degrees (e.g. if coils are double- and co-phasally fed, small model asymmetries can be compensated.).

An experimental unit with 1/10 output has so far been tested and used for model feeding (3.35, 3.36).

+) IPP report 4/29

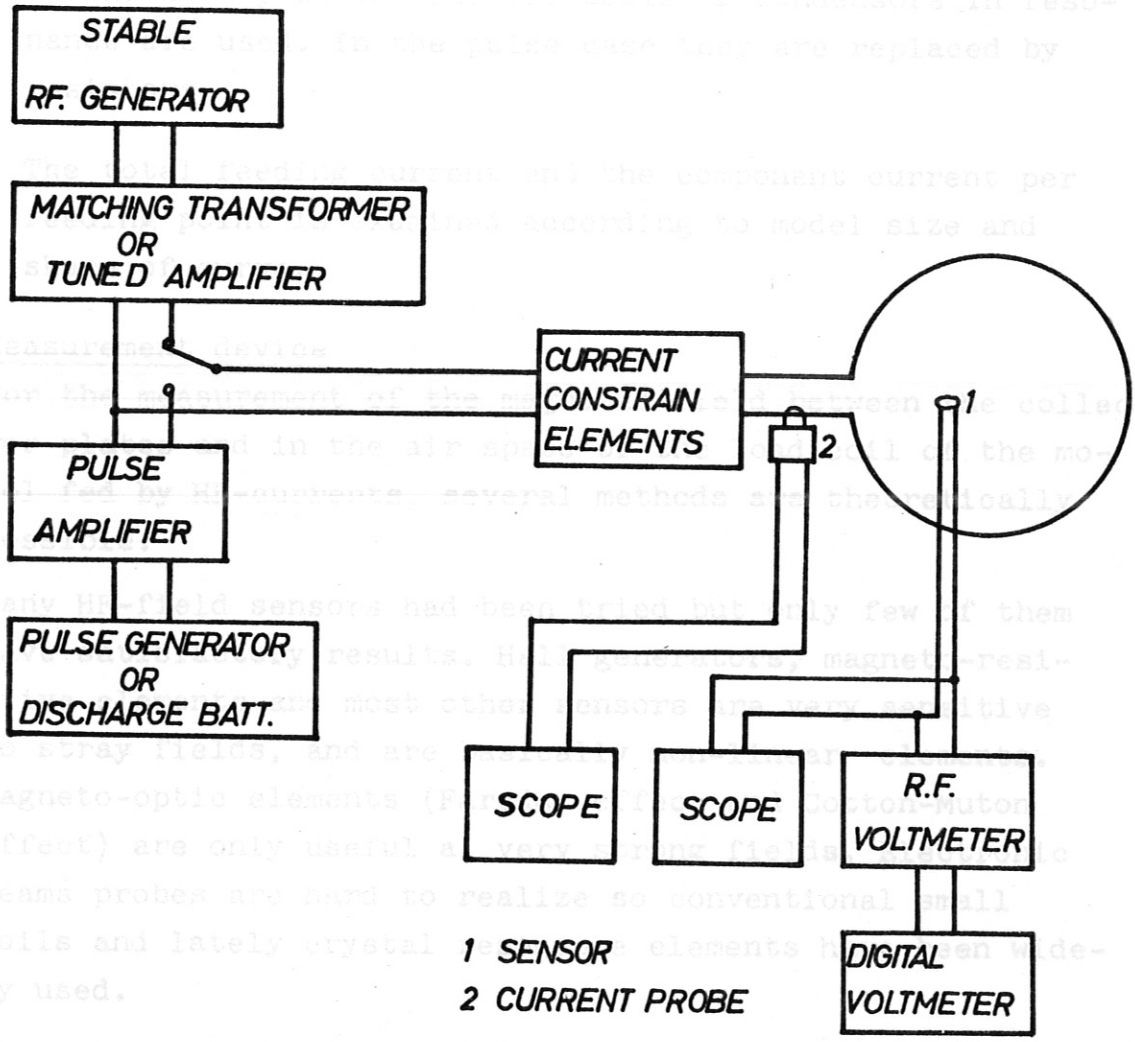

P 069 HF - fed models
feeding and measurement
device.

In order to simulate in the model a current distribution which corresponds to the actual one, constrain elements are used whose impedance is large compared to the model. In the steady state case air coils or condensors in resonance are used. In the pulse case they are replaced by resistors.

The total feeding current and the component current per feeding point is examined according to model size and shape of curve.

3. 3.3 Measurement device

For the measurement of the magnetic field between the collector plates and in the air space of the load coil of the model fed by HF-currents, several methods are theoretically possible:

Many HF-field sensors had been tried but only few of them gave satisfactory results. Hall generators, magneto-resistive elements and most other sensors are very sensitive to stray fields, and are basically non-linear elements. Magneto-optic elements (Faraday effect and Cotton-Muton effect) are only useful at very strong fields. Electronic beams probes are hard to realize so conventional small coils and lately crystal resonance elements have been widely used.

The output of the sensor (with proper convertor if necessary) is connected to a VTVM and oscilloscope. The scope is for showing the wave shape and the VTVM for exact measurement of the field value. In steady state case a tuned selective voltmeter can be used, while for pulsed models a broad band RF voltmeter must be used, preferably connected to a digital voltmeter.

3. 3.3.1 Coil probes

The dimensions of the probes must be as small as possible so that firstly the deformation of the field distribution, caused by the probe, remain small and secondly it is possible to measure the magnetic field between the collector plates. The probes used have the following data:

outside diameter 0.8 mm
axial thickness 1 mm
winding number 24

The coils are wound of varnished Cu-wire of a diameter of 0.03 mm on a nylon-thread or ceramic rod (stick) and fastened in a brass tube of a diameter of 1 mm; they are adjusted for measurement of a) the radial field and b) the axial field. The connectionwires of the probes are twisted andled to the shielded coaxial twin-contact jack, fastened at the end of the brass tube of a length of approx. 200 mm. In the area of the probe, the brass tube is slotted for suppressing interfering eddy currents.

3. 3.3.2 Measurement accuracy

Following factors are decisive for the measurement accuracy:

1. The stability of the input current.
2. The stability and selectivity of the measuring device.
3. The capacitive coupling of the probe to the model and its change during the course of the measurement.
4. The directivity pattern of the field sensor.

The influence of the first two sources of error can be kept below 0.1 per cent. Errors according to point 3 can be suppressed with the aid of the shielding (the brass tube). But up to now it was difficult to keep the directional distortion of the probe below 1 per cent. The directivity pattern of sensors will be measured more accurately in a special calibration apparatus.

3. 3.4 Copper model of the collector and the coil of the 1.5/2.6 MJ bank Isar I

3. 3.4.1 Aim of the measurement

Measurement of the coil field with coil probes in axial and radial direction.

3. 3.4.2 Models

The arrangement collector-sheet + coil of the project Isar I was constructed of copper sheet in the scale 1:5.

The region in front of the coil connection is provided with 150 slots (as performed on the original). For comparison, the measurements were also effected before slitting the conductor. For gaining equal feeding currents, an inductive resistance of approximately 10 Ω was inserted at each feeding point. (Picture P 035)

3. 3.4.3 Feeding

As a fitting amplifier has not been at out disposal, a HF generator was employed as power source with an output power of 30 kW and an invariable frequency. This generator is normally employed for inductive heating and therefore it is not very stable.

The total feeding current amounted, according to the experiments, to 100 A - 200 A. With this load, the frequency of the generator is approx. 500 kHz (by using a scale 1:5 and the original frequency of 25 kHz, the model nominal frequency would amount to 625 kHz.)

The series coils had to be cooled because of the high current density in the continuous operation. The current connection of the generator is combined with a cooling-water connection. The series coils were connected to this cooling circuit. (Picture P 035).

3. 3.4.4 Measurement results

The axial component of the magnetic field in the coil has been measured as a function of the coil length. Measuring channels were at the axis and at 4 positions along the inner periphery. The results show that the magnetic field distribution along the inner periphery is strongly influenced at the seperating lines between two coil segments. Deviations in magnetic field density up to 6% have occured. In a sectional plane normal to the coil axis field density eleviations of + 3,7 %, - 2,6 % have been determined. This plane was in the middle of a coil segment so that no influence of the separating lines occured. By reasons of symmetry the radial component

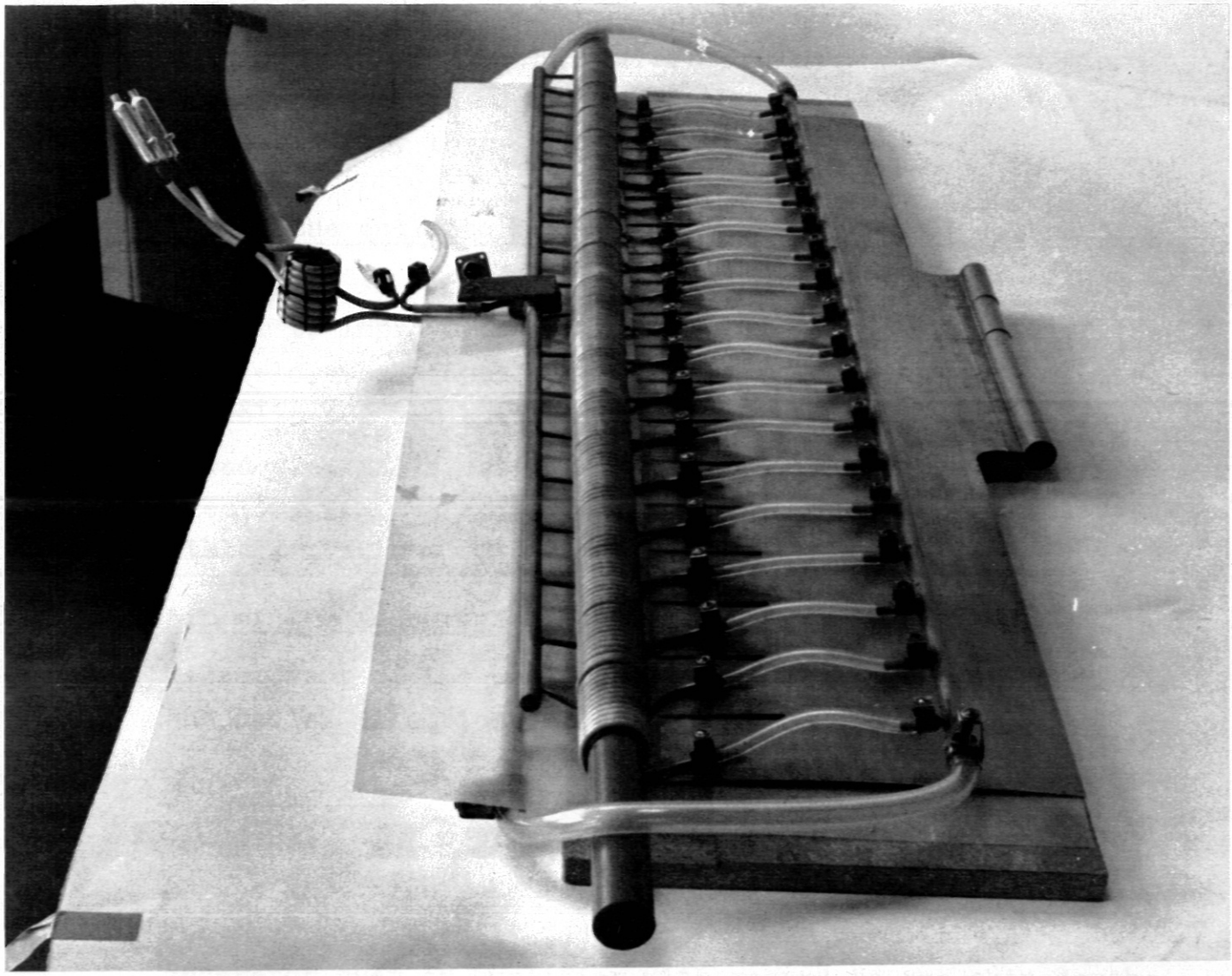

P 035 Scaled High Frequency Models
Model of Isar I - collector

of the magnetic field in the middle of the coil has to be zero. In this position however a signal which represents 0.6 % of the axial component has been measured. This signal is due to a direction error of the probe, which means radial components $\leq$ 0,6 % of the axial component can not be measured by this type of probes.

3. 3.5 Model of the collector extension in the 1.5/2.6 MJ bank Isar I

In order to improve the homogeneity and the symmetrie of the coil field, the adapter piece between the front edge of the main collector and the coil is extended. Thus the coil is removed from the steelplates and the lead masses of the main collector. A model was constructed for studying the influence of this provision.

3. 3.5.1 Aim of the measurement

Measurement of the coil field with coil probes in axial and radial direction.

3. 3.5.2 Model, feeding

In this spatial model built in the scale 1:4.5, the iron masses were also made to scale (picture P 030, P 031). The model is steadily fed with 500 kHz by a stable RF generator over an amplifier with regard to the skin depth; equal feeding currents were forced by series capacitances.

3. 3.5.3 Measurements results

In a first series of measurements the axial component of the magnetic field in the coil as a function of the coil length has been determined. At the seperation lines between two coil segments a field density deviation of $\pm$ 2,5% occured. If no attention is payed to the influence of the coil end and the separation lines the field density deviation in the whole coil volume is about $\pm$ 0.5 %. This deviation is below the accuracy of the used measuring device.

A comparision of the results from 3.3.4.4 and 3.3.5.3 shows that the collector extension entails a considerable

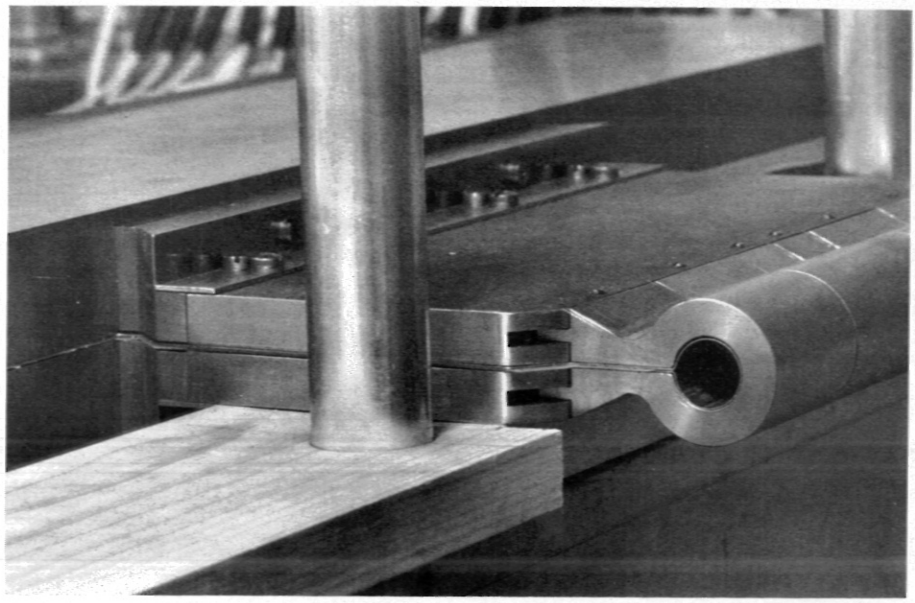

P 030 1,5/2,6 MJ - Theta-Pinch Isar I
Model of collector extension (detail)

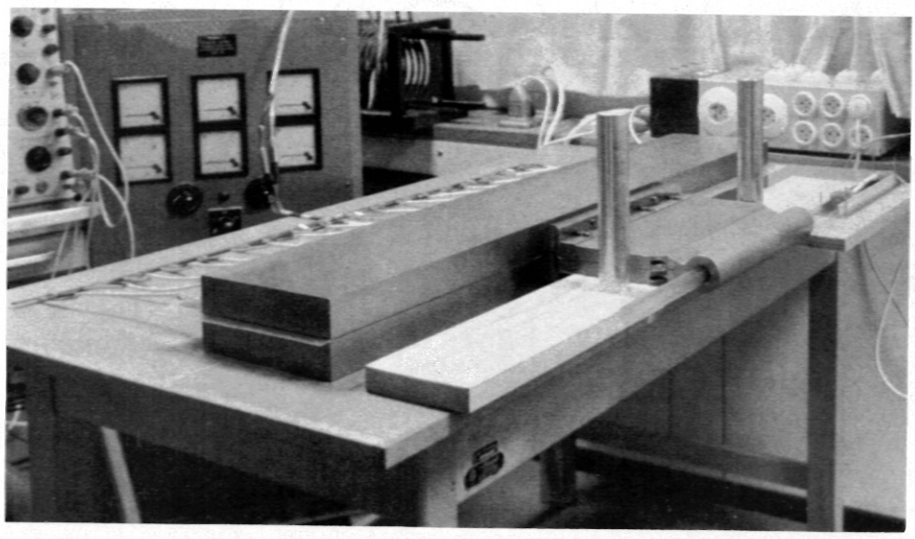

P 031 1,5/2,6 MJ - Theta-Pinch Isar I
Model of collector extension

improved homogeneity of the magnetic field distribution.

3. 3.6 Model of the double fed coil of the 10 kJ Turbulence Heating Experiment

3. 3.6.1 Double fed coil

A new principle was applied for the two capacitor banks which are at present under construction. The arrangement of the double fed coil is symmetrical about the two main plains of the coil; furthermore the series connection of two bank-halfs yields a high discharge frequency with a large stored energy. In the 10 kJ Turbulence Heating experiment, a separate multi-turn magnetic field coil surrounds concentrically the double-fed main coil (P 070).

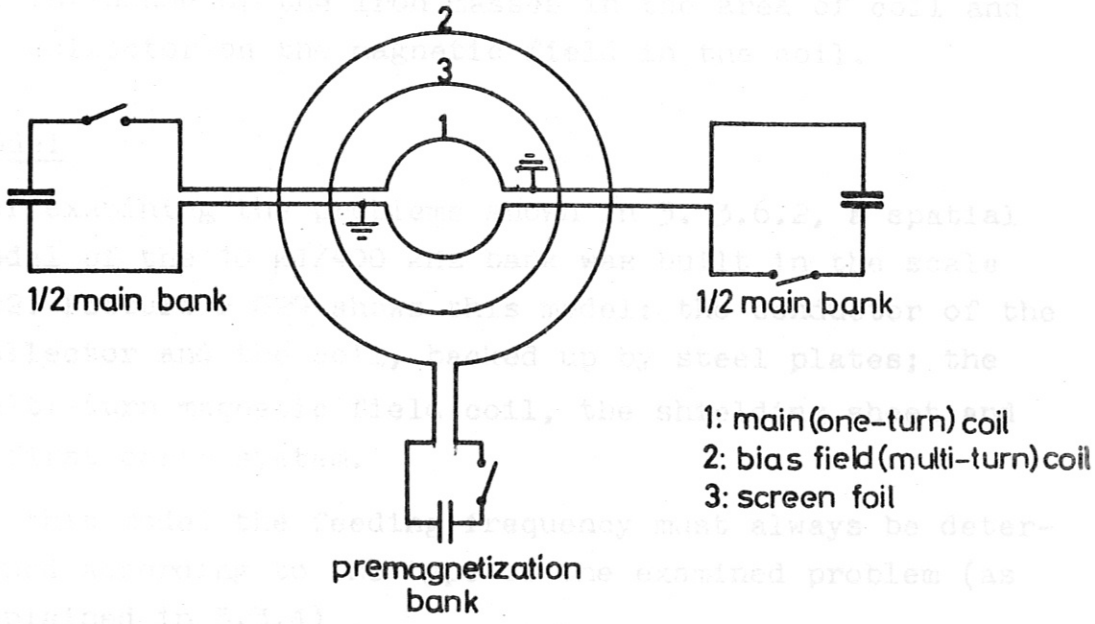

P070 Principle scheme of the Turbulence Heating Experiment

3. 3.6.2 Problems

For the realization of the new arrangement some questions must be cleared up:

1. Simultaneous switching of both banks, charged with the same voltage; examination of the effects if switching does not take place simultaneously.
2. Design of the dual earthing of the double-fed coil. The earth connection must be able to guide a large current if one of the bankhalfs is fired too late or only partially.
3. The fast discharge into the main coil induces voltages of 1000 kV or more in the multi-turn magnetic field coil. Therefore a field shielding must be provided between the two concentrical coils.
4. Influence of the iron masses in the area of coil and collector on the magnetic field in the coil.

3. 3.6.3 Model

For examining the problems shown in 3. 3.6.2, a spatial model of the 10 kJ/400 kHz bank was built in the scale 1:2. Picture P 029 shows this model: the conductor of the collector and the coil, backed up by steel plates; the multi-turn magnetic field coil, the shielding sheet and a first earth system.

In this model the feeding frequency must always be determined according to the type of the examined problem (as explained in 3.3.1)

The measurements are still going on.

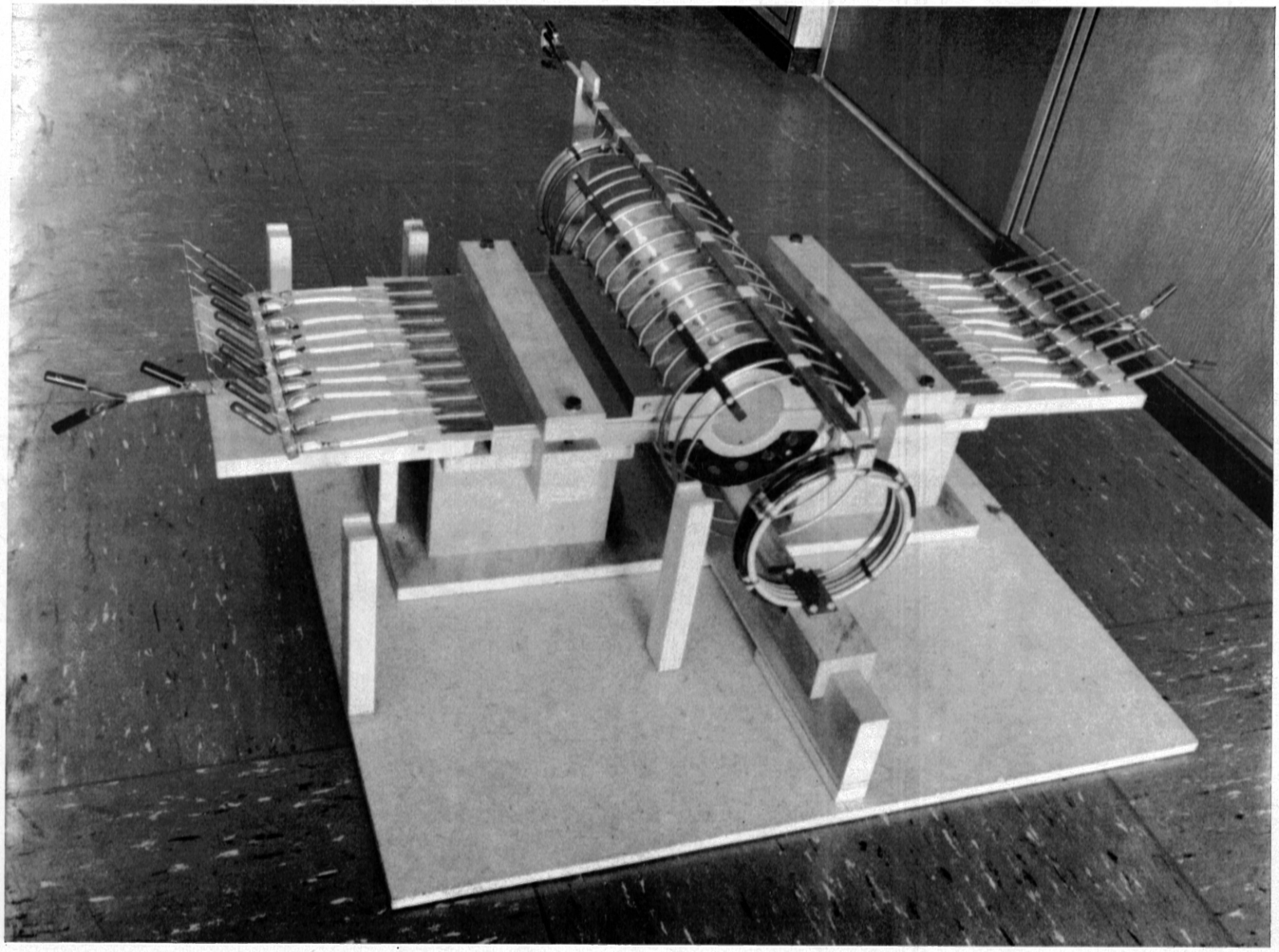

P 029 Turbulence Heating Experiment
Model of main and bias field coils

3.4 Spatial and surface potential distribution problems simulated in the electorlytic tank (F. Werner)

3.4.1 A model of the "Isar 1" collector made of insulated material

Usual arrangements of metallic conductors serve to produce high frequent magnetic fields of pretended geometric shape. The known relations between the geometric distribution of currents and the corresponding magnetic field, as expressed in the law of Biot-Savart, are not always applicable, because due to the inducing influence of the alternating magnetic field, the spatial current distribution is not known. Mainly however, the used frequency is in such order of magnitute, that the skin depth of the current in the metallic conductor is small in relation to the dimension of the air space in which the magnetic field should be produced.

The same is valid for the magnetic field, which means that the energy of the magnetic field inside the conductor is very small in comparison to the energy outside.

This screening effect of metallic surfaces against high frequency currents and fields supplies an especially simple method for the approximate determination of high frequent current distributions. This method is explained on the example of a relatively short solid coil.

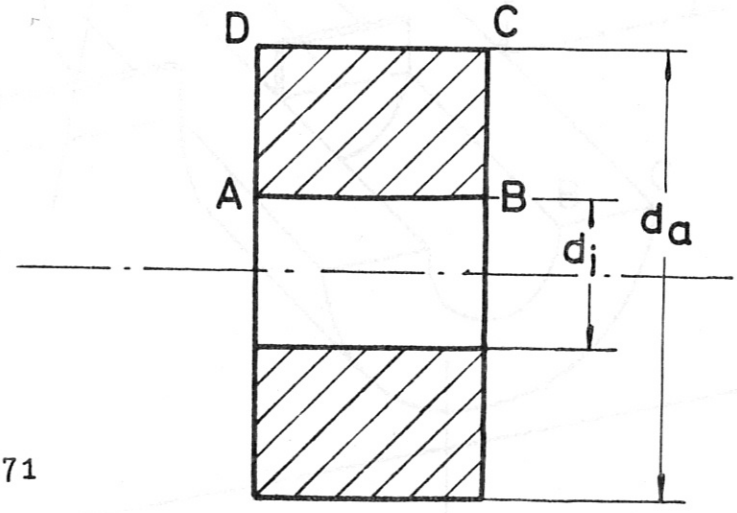

Fig. P 071

In this example the way of the real feeding is neglected. Furthermore it is provided that the coil is fed by a high frequent current which entails a skin depth $\delta \ll d$. Now one may assume that the main part of the current will flow on the inner region A-B, however a certain portion of current can be expected along A-D, BC and C-D. According to the condition $\delta \ll d$ the magnetic field energy will be mainly outside the cross section A-B-C-D of the metallic conductor, as a thin surface current zone is screening the inner part of the cross section. Neglecting displacement currents the high frequent magnetic field outside the conductor is at every time a potential field. If local phase displacements are disregarded the problem is reduced to the determination of the magnetic potential field around the screened cross section A-B-C-D.

This can be accomplished in the electrolytic tank by producing an analogue electrical potential field around a coil body which is made of insulating material. Electrodes representing the potential sheet are set in a plane of symmetry which is necessary for the analogue solution.

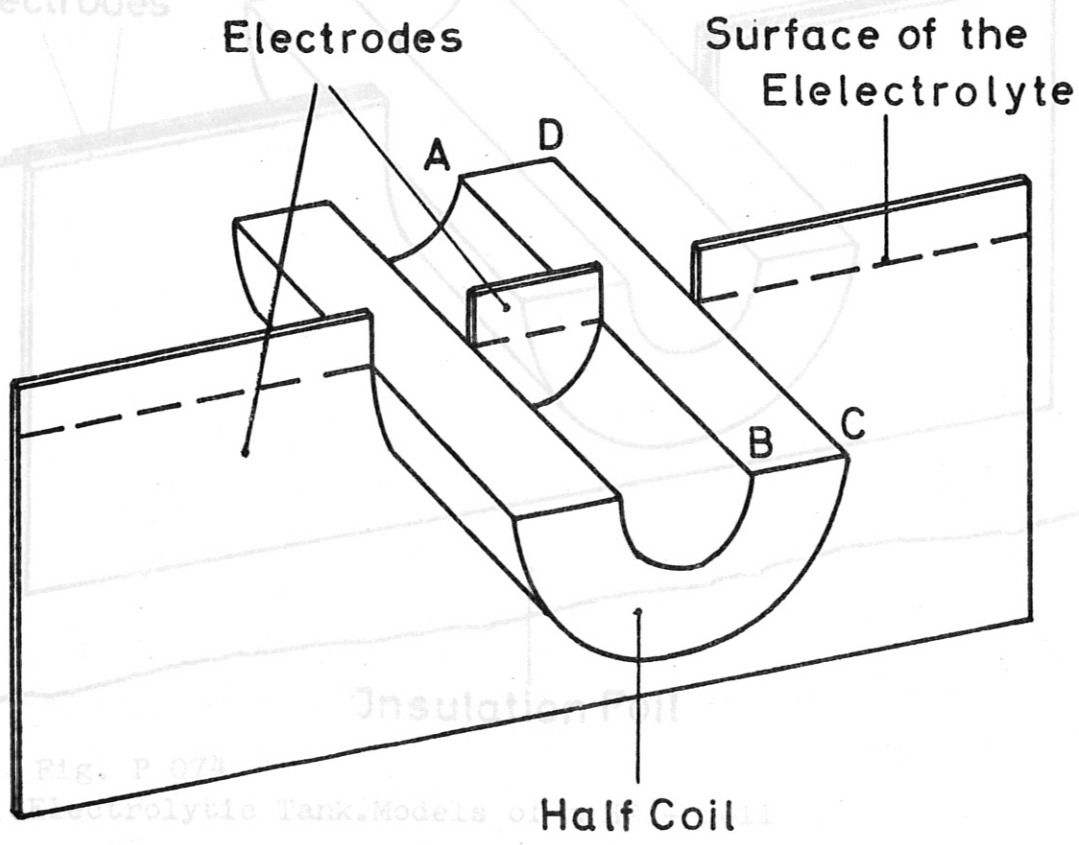

Fig. P 072

The voltage between the two electrodes corresponds to half the magnetic potential difference given by the total current.

The same measurement can be done by using double electrodes. In this case the voltage between the electrodes corresponds directly to the magnetic potential difference. (Fig. P 074)

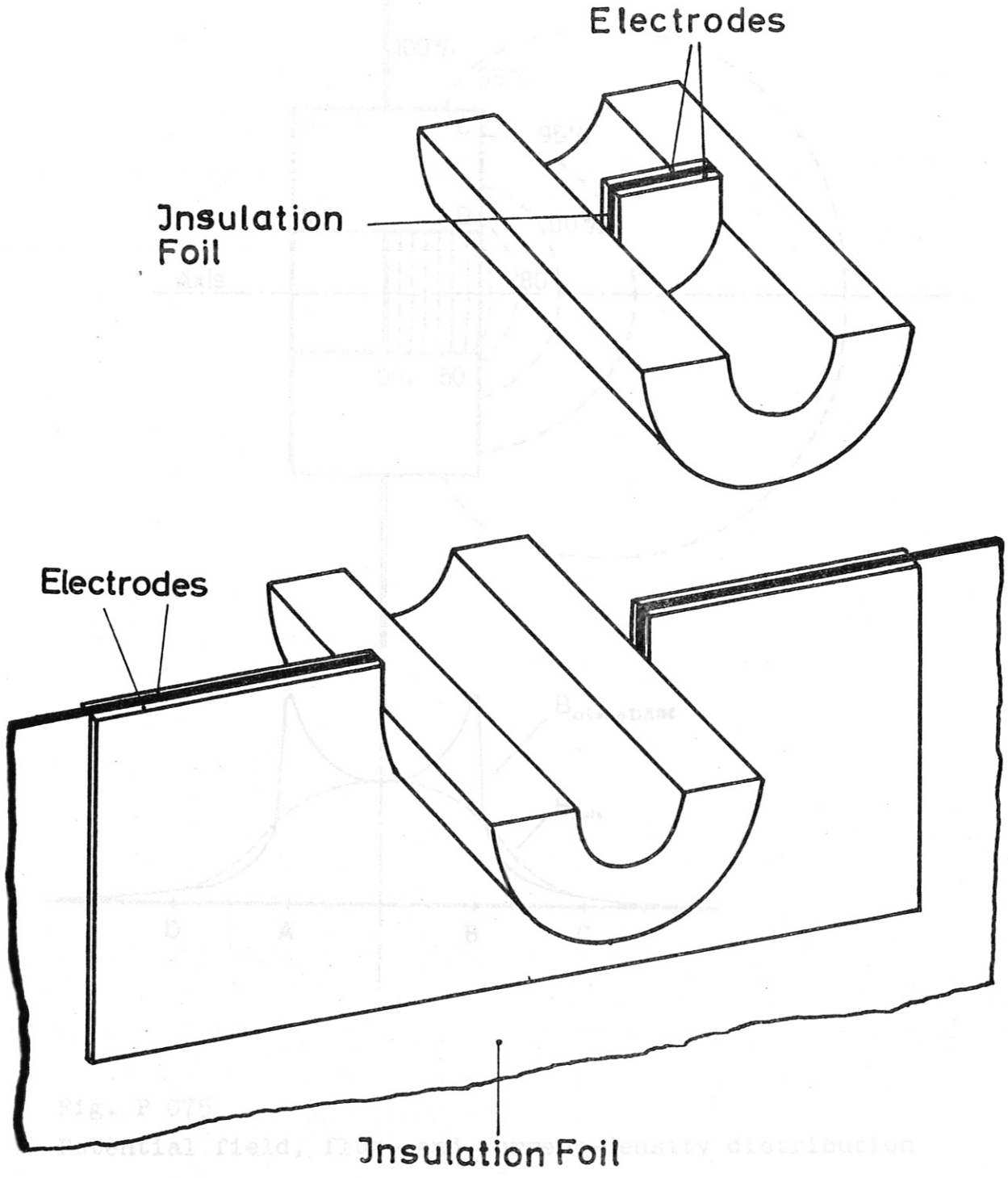

Fig. P 074
Electrolytic Tank. Models of a HF - coil

The picture of the resulting potential distribution supplies the approximate current density distribution along the cross section A-B-C-D by evaluating the tangential component of the magnetic field on the conductor surface. Fig. P 0 75 shows the determination on the previous coil model.

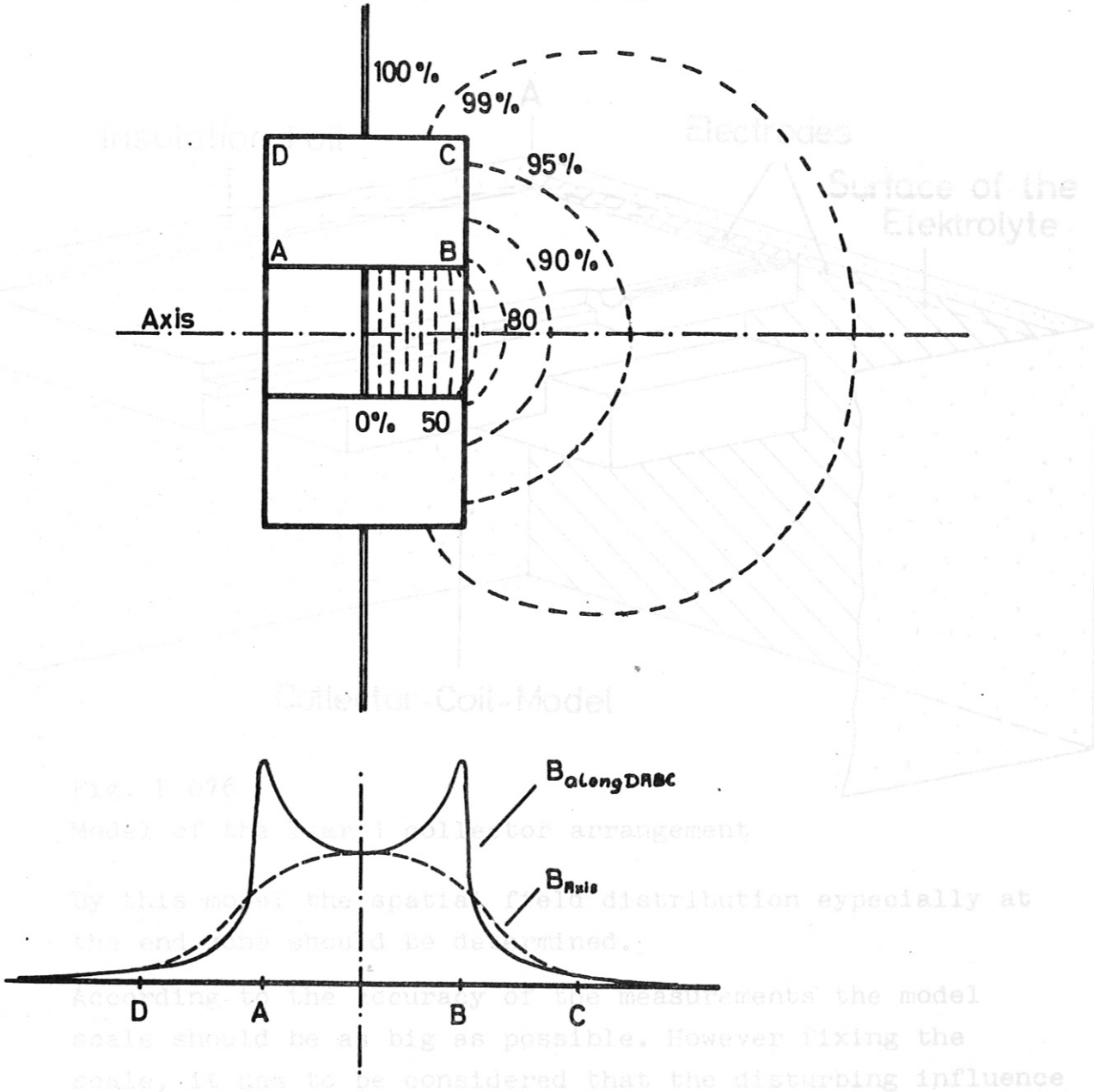

Fig. P 075
Potential field, flux- and current-density distribution

The shaded area in Fig. P 075 b supplies in combination with the known value of the total current a calibration of the current- and flux-density distribution.

In this way the collector coil arrangement of the "Isar 1" capacitor bank has been simulated by an insulating material model in the electrolytic tank (Fig. P 076).

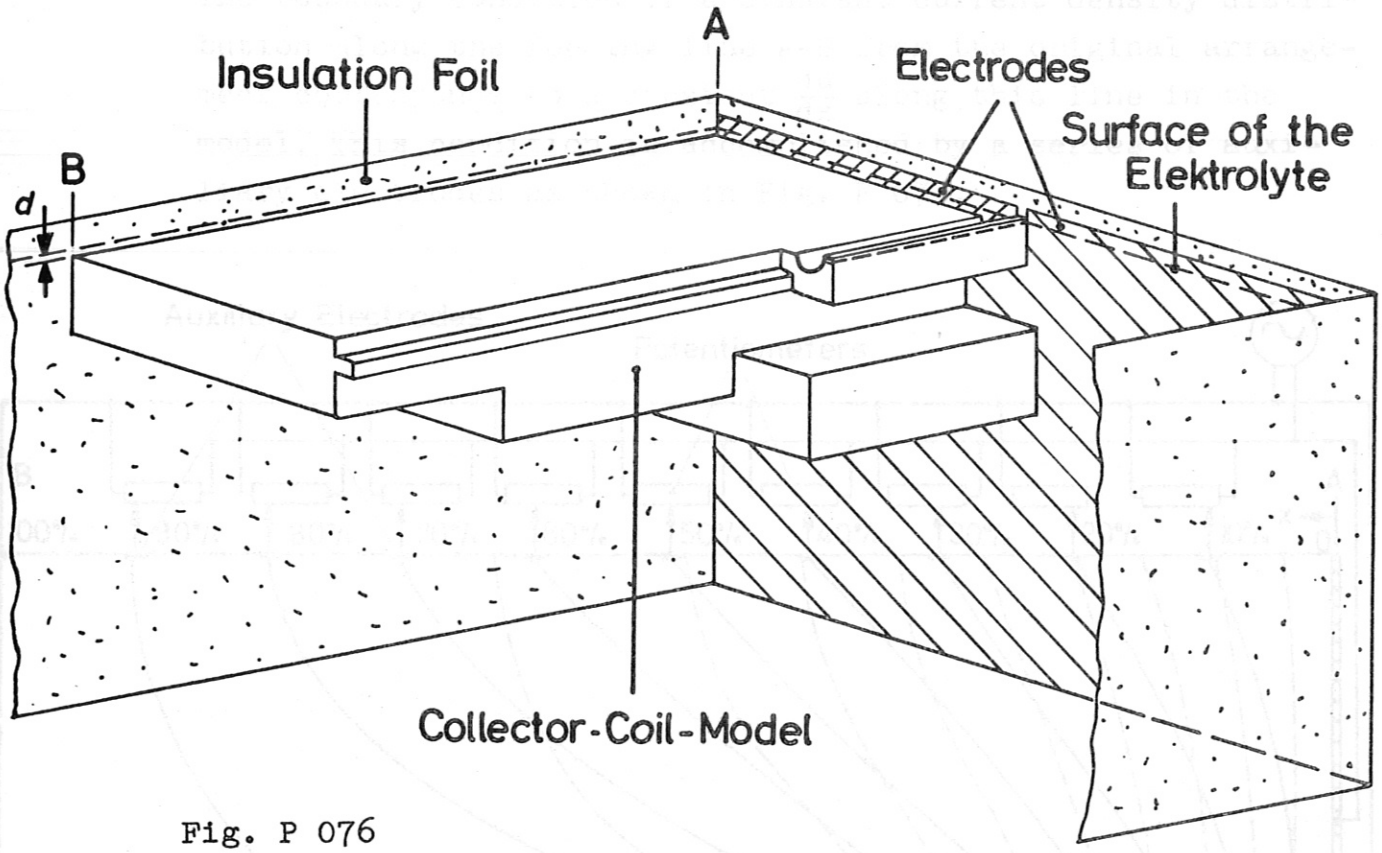

Fig. P 076
Model of the Isar 1 collector arrangement

By this model the spatial field distribution eypecially at the end zone should be determined.

According to the accuracy of the measurements the model scale should be as big as possible. However fixing the scale, it has to be considered that the disturbing influence of the tank boundaries to the field distribution is kept small. As the model could be cut in both planes of symmetry it simulates at least one quarter of the collector - coil arrangement so we could choose a model scale of 1/3. The field producing electrodes, which are connected to a 100

Volts / 400 cps power supply, are equipotential planes, located in the vertical plane of symmetry. The other plane of symmetry is the surface of the electrolyt, which in our case is tap water. Some difficulties were encountered with the realisation of the thin water layer in a constant depth over the collector area. The depth d is representing half of the distance between the two collector plates.

The boundary condition of a constant current density distribution along the feeding line A-B from the original arrangement corresponds to a constant $\frac{du}{dx}$ along this line in the model. This condition is accomplished by a series of auxiliary electrodes as shown in Fig. P 077.

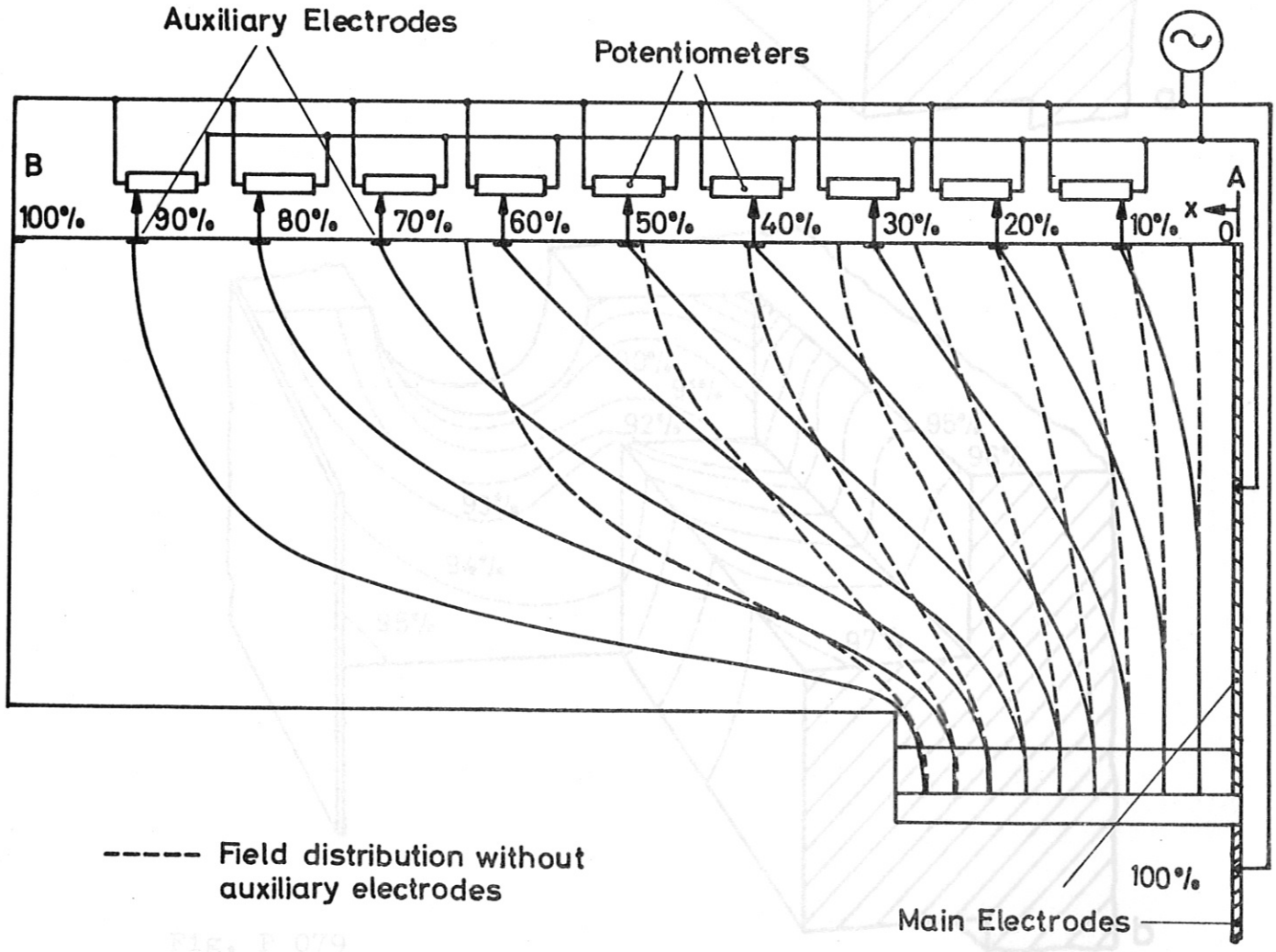

Fig. P 077 Boundary - conditions

Fig. P 079 a shows the potential distribution at the end zone of the coil.

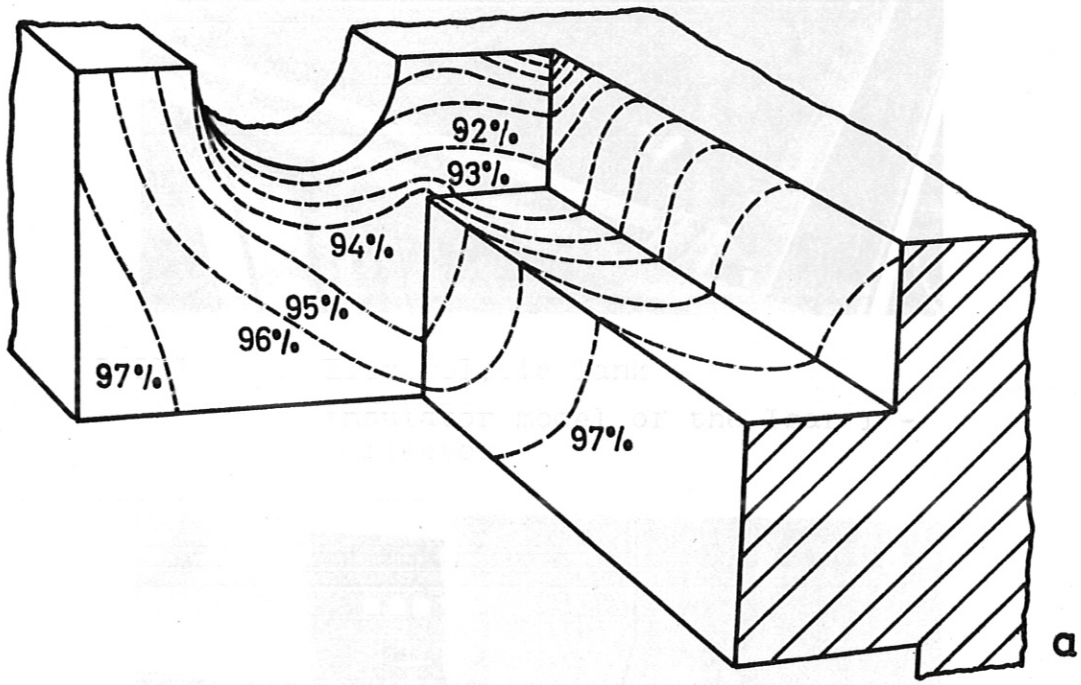

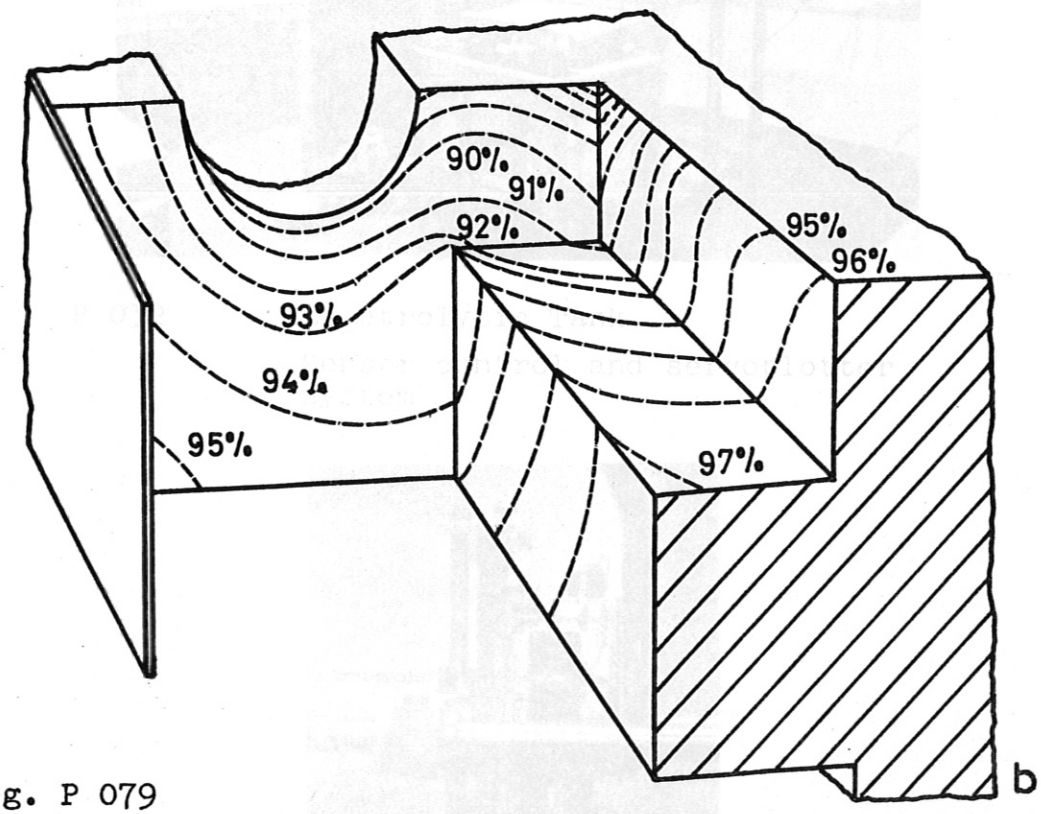

Fig. P 079

Electrolytic Tank.

Model of the Isar I collector arrangement.
Potential distribution at the end of the coil.

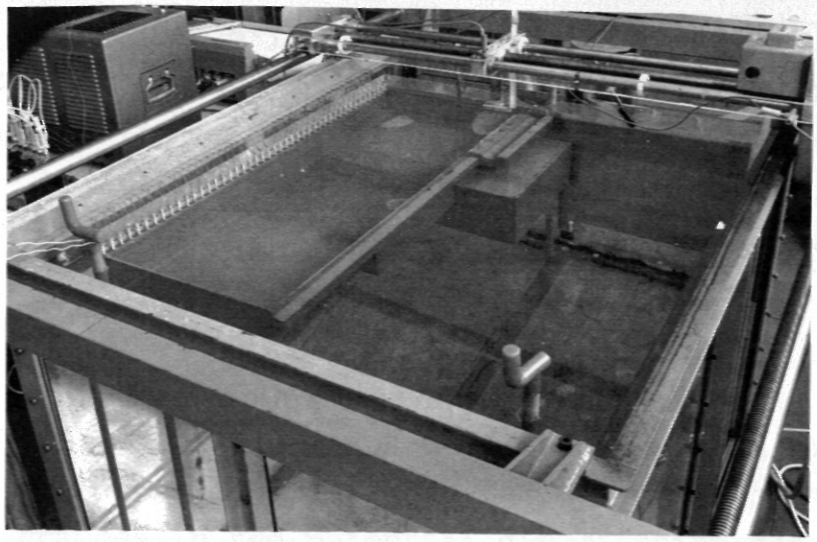

P 034 Electrolytic Tank

Insulator model of the Isar I - collector

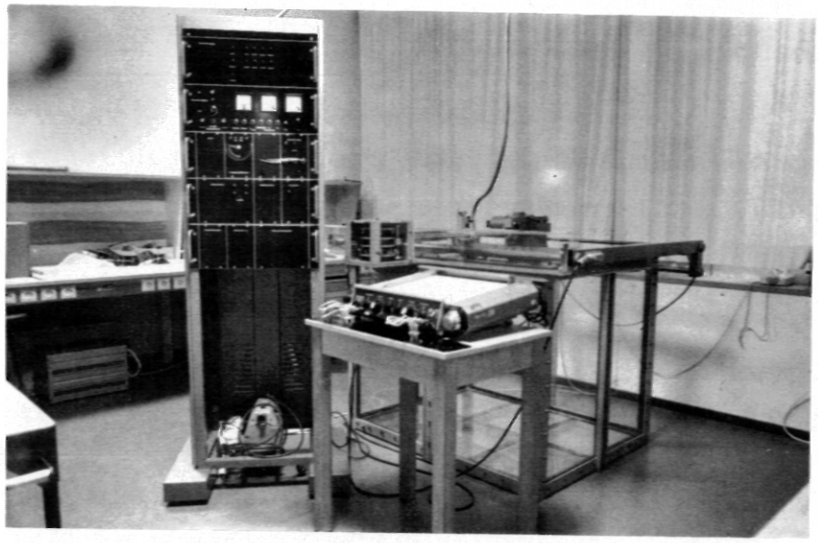

P 032 Electrolytic Tank

Sensor control and servoplotter system

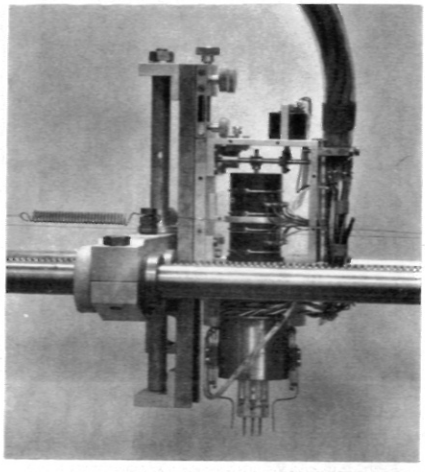

P 033 Electrolytic Tank

Sensor including probes, component splitter and angular position motor

In order to increase the symmetry of the magnetic field distribution (to the coil axis) a screening metal sheet added to the coil as shown in fig. P 079 b. The effect of improving the symmetry is demonstrated by comparision of fig. P 079 a and P 079 b.

3. 4.2 The servo plotter system

The manual plotting of equipotential lines in an electrolytic tank can be a very laborious and tedious process. Moreover to avoid changes in the potential distribution due to the evaporation of the electrolyte, transient electromechanical and thermal effects, etc., it is desireable to accomplish the measurements as rapidly as possible.

By these reasons a servo plotter system has been developed and built.

Two DC-direction motors, one moving in the x - and one in the y - direction shall lead a sensor at constant velocity along an equipotential line. That means the velocity has to be in a tangential direction to the line.

This is realized by controlling the direction motors, corresponding to the direction of the line, with the sin φ - and cos φ - components of a constant voltage U_{tang} (Fig. P 080)

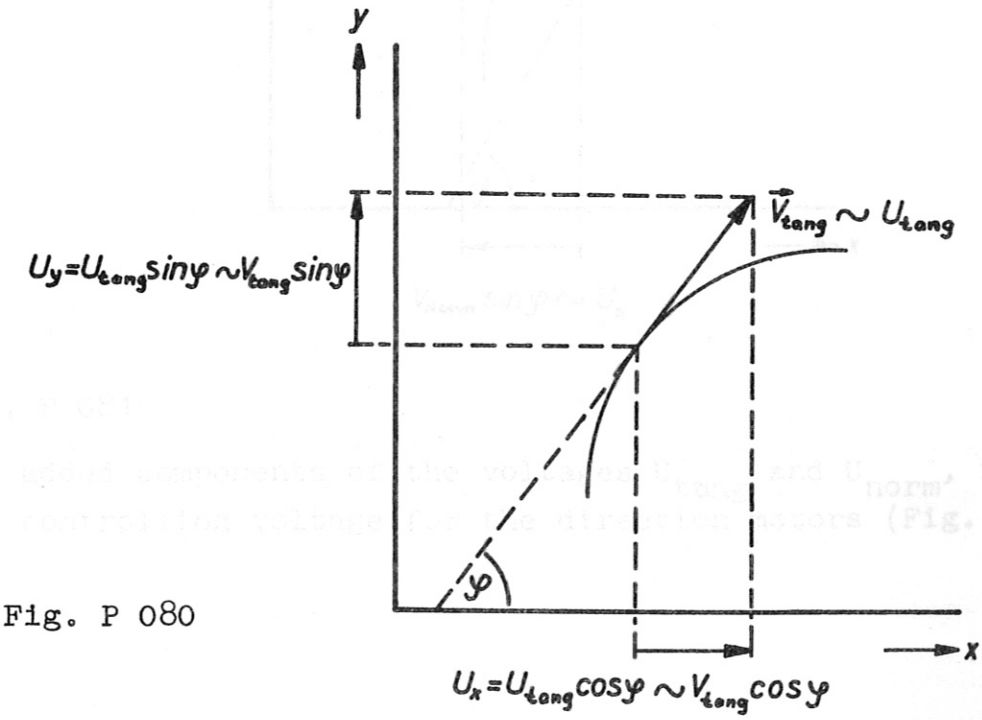

Fig. P 080

The sensor bears three measuring pins (S_1, S_2, S_3) of which the two outer ones control the angular position of the probe head. The voltage U_{rot} between S_1 and S_3 controls a position motor which rotates the sensor and the components splitter about their own axis until the input signal from the two outer pins is zero. The probe head is then orientated along an equipotential line.

For tracing a certain equipotential line the central pin S_2 is used.

The potential difference U_{norm} between S_2 and the potential U_o of the desired line, which is selected by a reference voltage selector, has to control both of the direction motors in a way that the sensor gets a velocity normal towards the equipotential line.

This is accomplished by splitting U_{norm} in its $\sin\varphi$ and $\cos\varphi$ components as shown in fig. P 081.

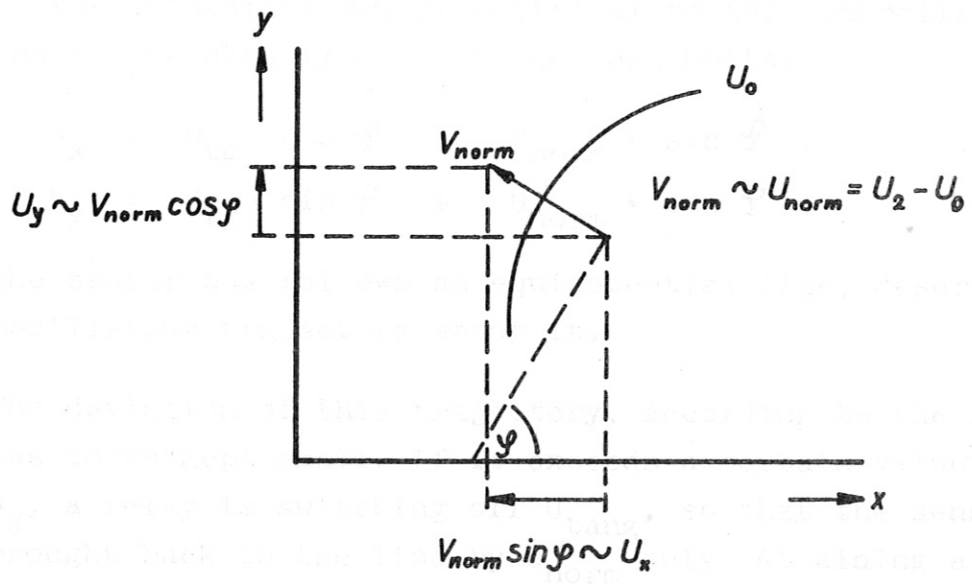

Fig. P 081

The added components of the voltages U_{tang} and U_{norm}, form the controlling voltage for the direction motors (Fig. P 082)

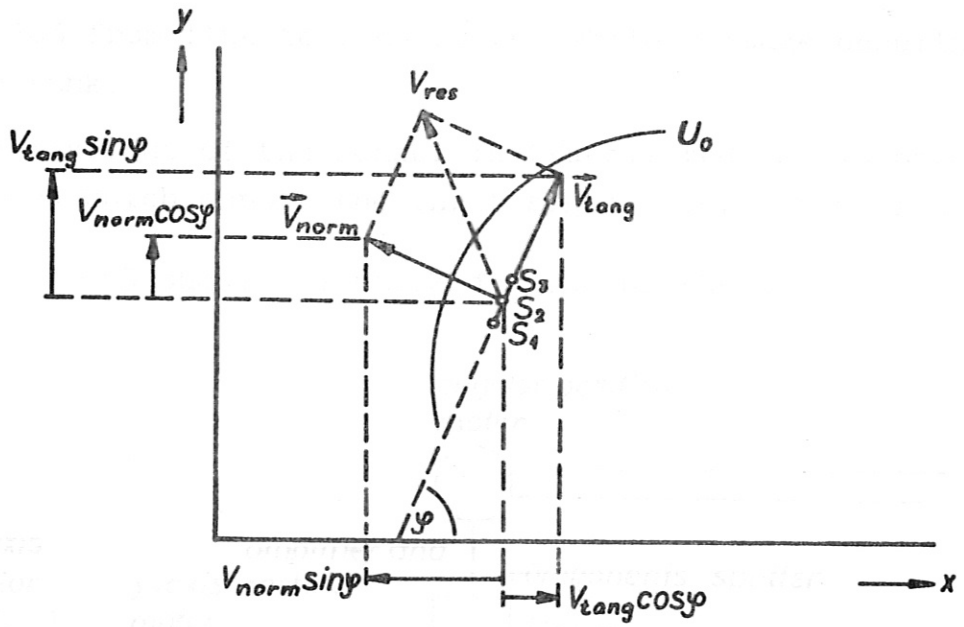

Fig. P 082

$$\vec{V}_{res} = \vec{V}_{tg} + \vec{V}_{norm}$$

$$V_x = |\vec{V}_{tg}| \cdot \cos\varphi - |\vec{V}_{norm}| \cdot \sin\varphi \quad ;$$

$$V_y = |\vec{V}_{tg}| \cdot \sin\varphi + |\vec{V}_{norm}| \cdot \cos\varphi \quad ;$$

As the velocities are proportional to the controlling voltages of the direction motors one can write:

$$U_x = U_{tg} \cdot \cos\varphi - U_{norm} \cdot \sin\varphi \quad ;$$

$$U_y = U_{tg} \cdot \sin\varphi + U_{norm} \cdot \cos\varphi \quad ;$$

The sensor now follows an equipotential line, describing an oscillating trajectory about it.

The deviation of this trajectory, according to the accuracy has to be kept small. If it exceeds a certain value of $U_o - U_2$, a relay is switching off U_{tang}, so that the sensor is brought back to the line by U_{norm} only. Attaining a boundary a relay system switches off U_{tang} and U_{norm} until the sensor, now following the boundary, discovers the desired equipotential line again. If the sensor reaches its start position, which is stored mechanically, the reference voltage relay changes over to the next potential.

In this way a potential field can be plotted in steps of 5%

or 1o% from line to line of the whole voltage occuring in the tank.

The movement of the sensor is transmitted on two potentiometers which supply the input signals for a x-y-plotter.

Fig. P 083 shows the block diagram of the system.

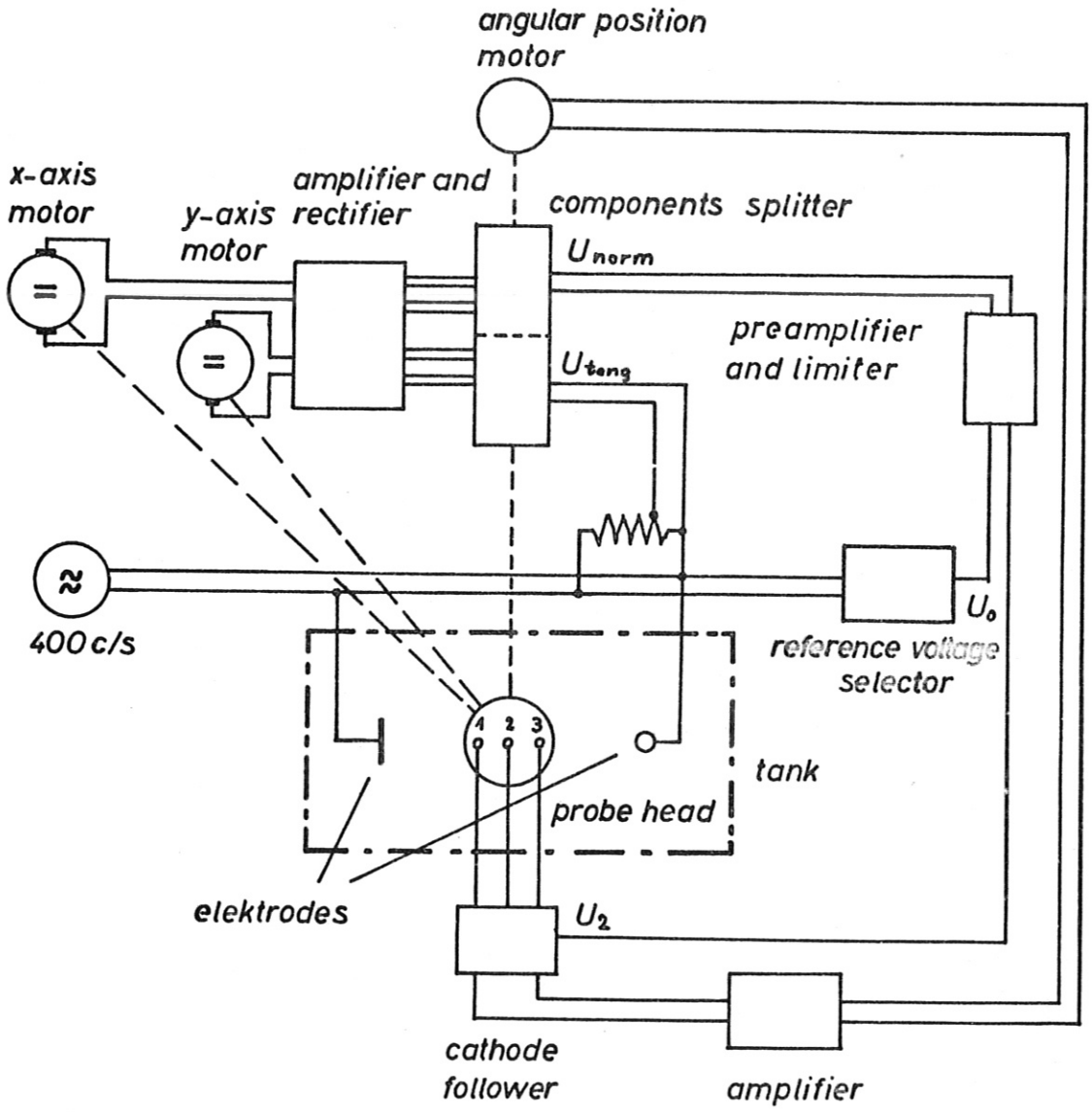

SYMBOLS : —— electrical connections

– – – mechanical connections

Fig. P 083

Acknowledgement:

The principle design of this system has been developed by Mr. Jean Deleplanque a former member of the technical department.

3. 4.3 The electronic equipment (G. Roos)

The above mentioned functions of the plotter system are realized by a complex electronic apparatus. Each of the different units are built in a rackmount plug-in and powered by a central supply.

3. 4.3.1 Probehead and impedance transformer

Three probes touch the surface of the electrolyte in the tank and sense the local electric potential of the liquid at their respective position. If there flows any remarkable current to the probes the field configuration may be disturbed giving an untrue result.

To avoid this, the input impedance of the probes must be very high over a large voltage range, as it should be possible to work with supply voltages for the tank up to 100 V.

Another difficulty is to make equal the loss of signal voltage in two channels, because the wanted signal is the difference of two voltages, which is very low compared with the voltages. (If the field distribution for example is linear, the maximum differential voltage, that can occur, is the same fraction of the supply voltage, as the geometric distance of the probes is a fraction of the space between the electrodes). To overcome this difficulties, we developed a special bootstrapped version of a cathode follower with a gain very close to one. The higher voltages in the tank call for vacuumtubes instead of transistors. The circuit is shown in fig. P 084.

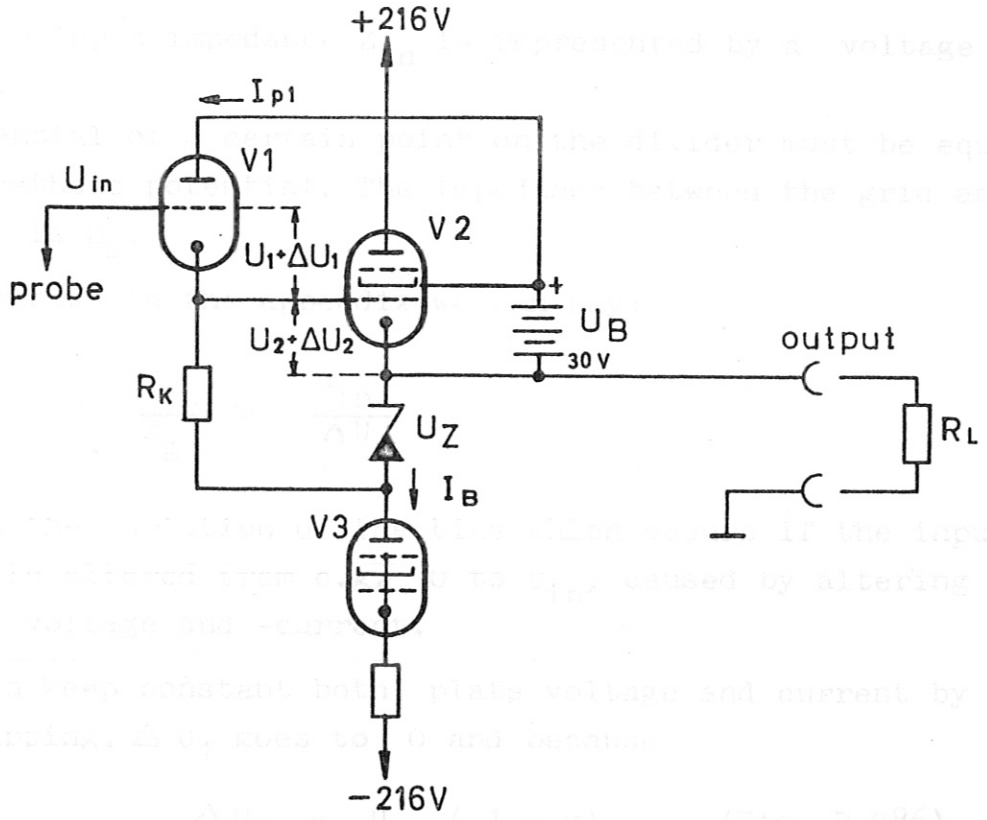

Fig. P 084

V_1 is a nuvistor, V_2 and V_3 are AF power tubes. V_1 and V_2 work as cathode followers, V_3 as constant current supply. U_B is a stabilized floating dc-voltage derived from a well insulated transformer winding. If we assume V_1 as an ideal tube with an infinite input impedance and keep constant the voltages at the tube, we can express the sum of all the currents flowing from or to the grid connection (such as residual, ion- and leakage currents to the other electrodes, reactive currents caused by the input capacity) by a grid impedance Z_g, which is connected between grid and cathode (Fig. P 085).

If we further neglect the dc-grid-bias U_1, this circuit is equivalent to the version of Fig. P 086.

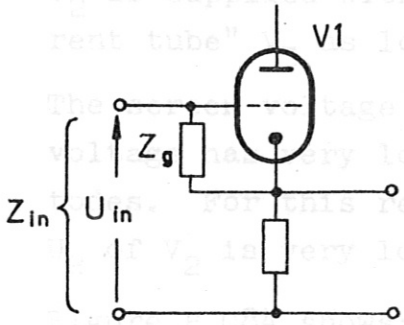

P 085

≡

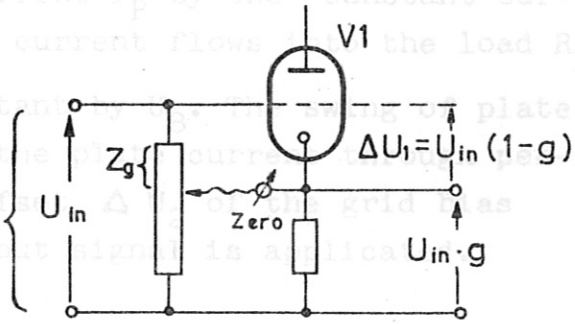

P 086

Here the input impedance Z_{in} is represented by a voltage divider.

The potential of a certain point on the divider must be equal to the cathode potential. The impedance between the grid and this tap is Z_g.

As also shown in the appendix we can say:

$$\frac{Z_{in}}{Z_g} = \frac{U_{in}}{\Delta U_1}$$

ΔU_1 is the variation of the bias which occurs if the input voltage is altered from e.g. 0 to U_{in}, caused by altering of plate voltage and -current.

If we can keep constant both, plate voltage and current by bootstrapping, ΔU_1 goes to 0 and because

$$\Delta U_1 = U_{in} (1 - g) \qquad \text{(Fig. P 086)}$$

((1-g) is the "loss of gain")
the gain g approaches to 1

Realizing this we overcome all problems:

1.) high input impedance
2.) gain near unity, therefore sufficient equal in different channels
3.) great voltage range allowable without lowering the input impedance

First we choose an operating point of V_1 like an electrometre tube with low plate voltage and current and reduced filament voltage in order to keep grid current low, then we bootstrap V_1 by the pentode V_2.

V_2 is supplied with constant current I_P by the "constant current tube" V_3 as long as little current flows into the load R_L.

The screen voltage is kept constant by U_B. The swing of plate voltage has very low effect on the plate current through pentodes. For this reasons the offset ΔU_2 of the grid bias U_2 of V_2 is very low when an input signal is applicated.

Figure P 084 shows:

Plate voltage of V_1: $V_{P1} = U_B - U_2 - \Delta U_2$; $U_B \gg \Delta U_2$

Plate current through V_1: $J_{P1} = \frac{U_Z + U_B + \Delta U_2}{R_K}$; $U_Z \gg \Delta U_2$

The effect of ΔU_2 upon V_{P1} and J_{P1} is strongly reduced by the addition of the large constant amounts U_B and U_Z to ΔU_2.

We can say J_{P1} and V_{P1} are practically constant therefore ΔU_1 is very low and we get:

$$Z_{in} \gg Z_g \quad ; \quad g \approx 1$$

We measured at the 3 impedance transformers built into the rack (worst case) the following spezifications:

V_1 : 7586 V_2, V_3 EL 81

max swing of input voltage U_{in} : - 198 ... + 200 V
pass band (- 3db) : 0 ... 10,5 kc/s (R_{gen} = 10 MΩ)
Input capacity: ~ 1 pF
Input resistance
R_{in} : > 5 . $10^{10}\Omega$ (grid open)
Input current (dc) : $\leq 4.10^{-11}$A (U_{in} = -160 V... + 160 V)
Total gain g : 0,9924 ($R_L \geq$ 100 kΩ)
noise: 25 mV (hum 50 c/s; Re = 10 MΩ)

The input stages (V 1) of the 3 impedance transformers are housed in a little cylindrical case and shielded from each other. The bottom made from plexiglas bears 3 miniature sockets to plug-in the probes. 3 flexible shielded cables carry supply- and output voltages to the chassis in the rack, which contents the rest of the circuit.

3. 4.3.2 Angular position system (Fig. P 087)

The probe head and the shaft of the component splitter are rotated by a 400 c/s 2 phase motor. The excitating winding of the synchro is powered with 400 c/s voltage shifted by a capacitor in phase quadrature to the supply voltage of the tank; the control winding is fed by a servo amplifier.

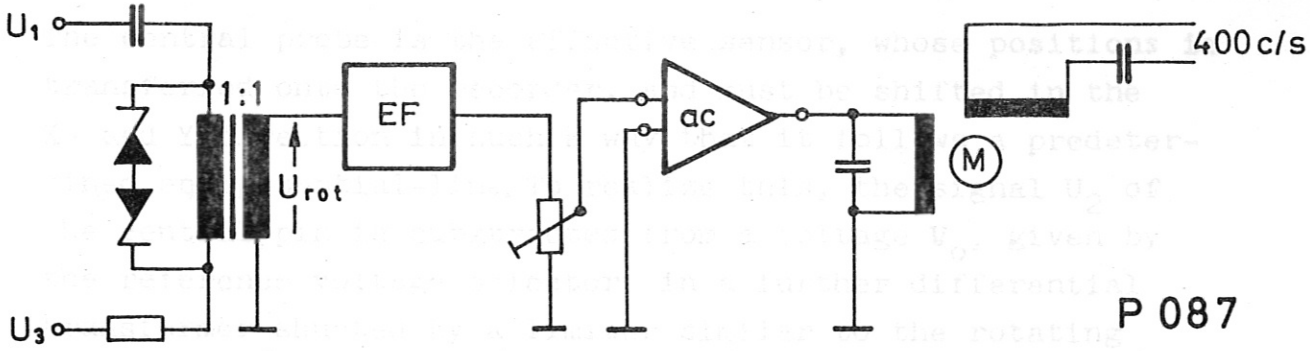

The difference of the signals U_1 and U_3 from the outer probes (U_{rot}) controls rotating of the probe head.

U_1 and U_2 are sub/tracted from each other in a differential transformer whose secondary winding is connected to the input of an ac-amplifier. To keep away overload from the input transistor, two oppositely polarized zener-diodes shunt the primary of the transformer. The input impedance of the amplifier is increased by an emitter-follower. The signal is amplified in 2 stages and a final power stage and fed into the control winding of the motor. Amplifier, servomotor, gear, probehead and tank form a control system, that adjusts itself for $U_{rot} = 0$. The sensitivy can be adjusted by a gain-control potentiometer to limit the loop gain of the system to a value, where no oscillations occur.

3. 4.3.3 Linear shifting system (Fig. P 088)

Preamplifier and limiter

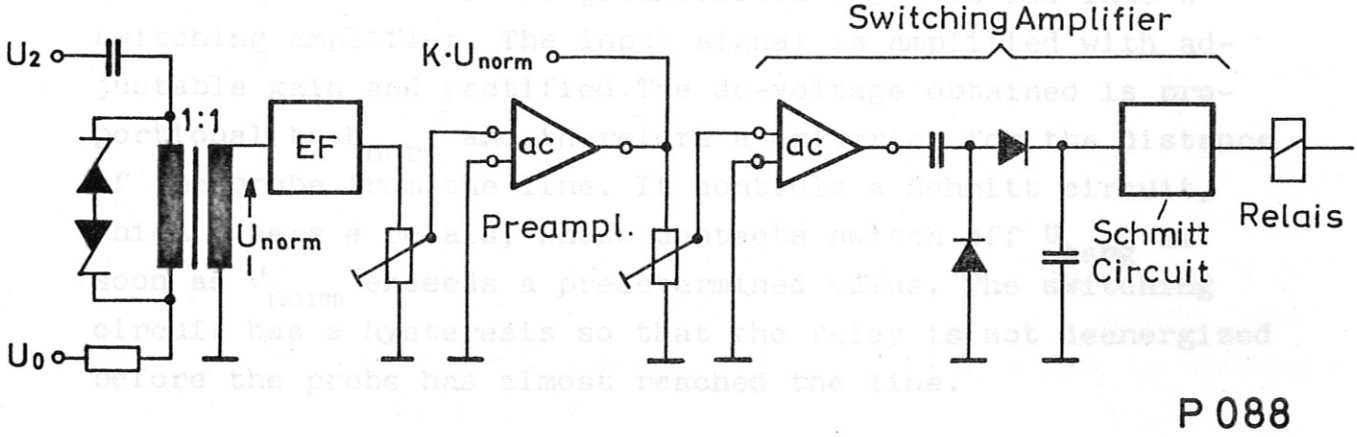

The central probe is the effective sensor, whose positions is transferred onto the recorder, and must be shifted in the X- and Y-direction in such a way that it follows a predetermined equipotential-line. To realize this, the signal U_2 of the central pin is subtracted from a voltage U_o, given by the reference voltage selector, in a further differential transformer shunted by a limiter similar to the rotating system. The voltage in the secundary winding, U_{norm}, is amplified and limited in a preamplifier with adjustable gain. Limiting is simply achieved by overloading the final stage. The output signal is branched into 2 ways:
to a switching amplifier, mounted on the same chassis and to the component splitter.

Sin- and cos-splitter

This is a precision potentiometer with a cos-characteristic. Two 90° staggered outputs deliver $\frac{U_{norm}}{2} \cdot \sin\alpha$ and $\frac{U_{norm}}{2} \cos\alpha$, where α is the angular position of the pot's shaft. A second identical potentiometer fixed on the same shaft splits the constant voltage U_{tang} into $\frac{U_{tang}}{2} \sin\alpha$ and $\frac{U_{tang}}{2} \cos\alpha$, producing the velocity tangential to the line.

Switching amplifier (Fig. P 088)

When the central probe S2 moves too far from the selected potential-line, it is driven back to the line by switching off U_{tang}, so that the motors are controlled by U_{norm} only.

The second branch of the preamplified U_{norm} is fed into a switching amplifier. The input signal is amplified with adjustable gain and rectified. The dc-voltage obtained is proportional to U_{norm} and therefore a criterion for the distance of the probe from the line. It controls a Schmitt circuit, which powers a relais, whose contacts switch off U_{tang} as soon as U_{norm} exceeds a predetermined value. The switching circuit has a hysteresis so that the relay is not deenergized before the probe has almost reached the line.

Power amplifier for X- and Y-direction motors

(Fig. P 089)

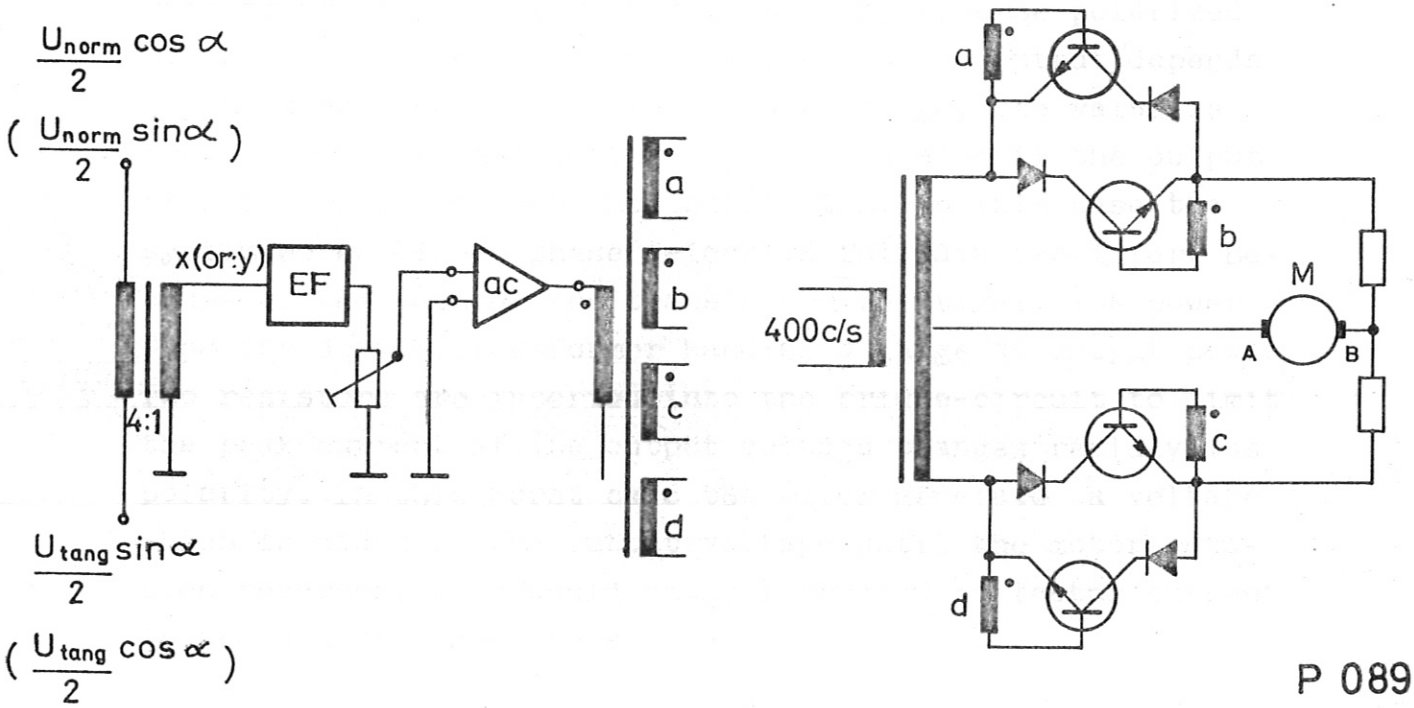

P 089

The motors for shifting the probe-head are both dc shunt motors with the field coils supplied with constant dc voltage. The armatures are fed from two identical power-amplifiers with dc output, mounted on one chassis. The input signals are derived from the component splitter. The difference

$\frac{U_{tang}}{2}\sin\alpha - \frac{U_{norm}}{2}\cos\alpha$ represents the X-movement

$\frac{U_{tang}}{2}\cos\alpha - \frac{U_{norm}}{2}\sin\alpha$ the Y-movement

The input transformer subtracts the components. Its turns ratio is 4 : 1 to prevent the component splitter being loaded by the input impedance of the input emitter follower. The 2 stage-amplified X or Y signal feds a driver transformer whose 4 insulated secundary windings are connected between base and emitter of 4 npn transistors which form a bridge circuit together with 4 silicon diodes and the center tapped supply transformer. The armature of the dc-motor is connected across the bridge-circuit. The input signal is in phase or in phase opposition to the 400 c/s supply voltage.

Therefore during each halfwave one of the 4 transistors is conducting, two of the others are cut off by reverse base-emitter-voltage; the last one has no collector voltage. This transistor is prevented from being reverse polarized by the series diode. The polarity of the dc-output depends on the phase position of the input voltage, the value is roughly proportional to the input voltage until the output transistors are driven into saturation. In this case the system works like a phase selective fullwave rectifier. Because of the gain of the transistors relatively low power from the driver transformer handles a large dc output power. Two resistors are inserted into the bridge-circuit to limit the peak current if the output voltage changes rapidly its polarity. In this worst case the motor generate a voltage which is added to the output voltage until the motor rotation reverses, this would cause increased collector current in the output transistors.

Monitoring unit (Fig. P 090)

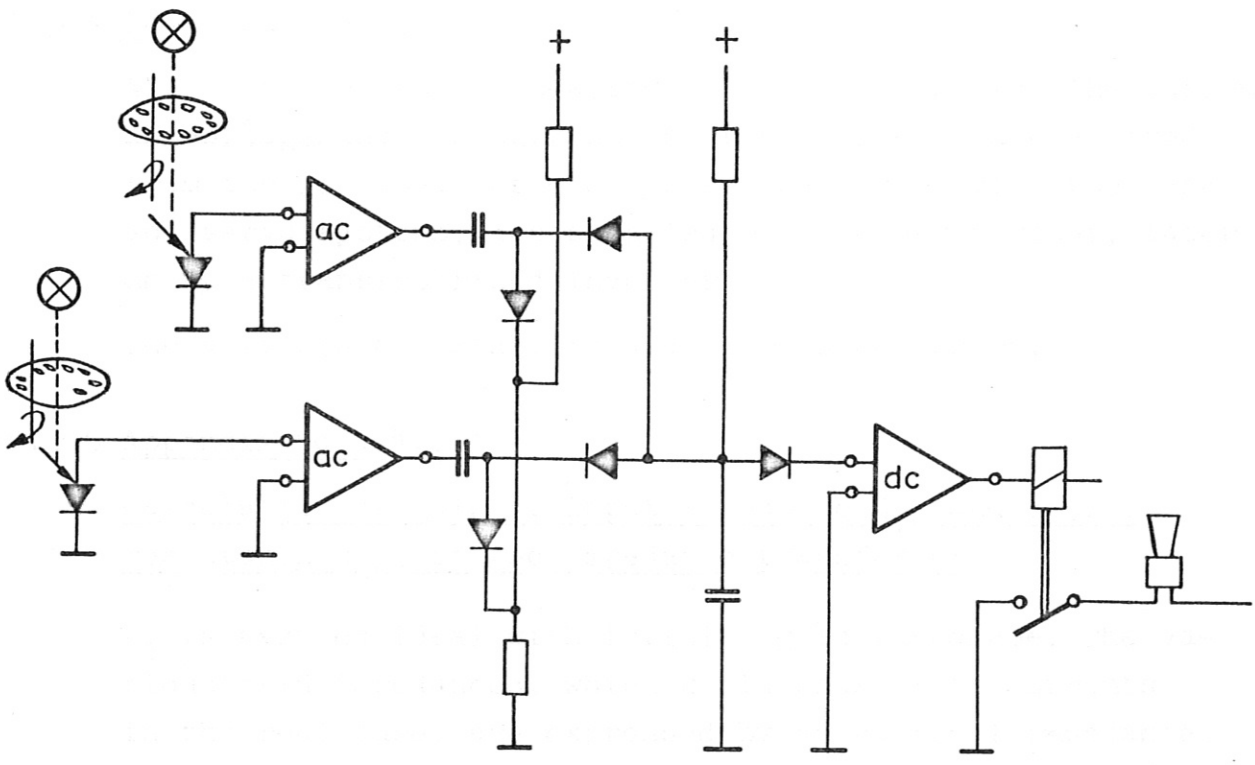

P 090

It is necessary to monitor the automatic plotting system and to call for the operator by an acoustic signal in the case of standstill.

This is made by looking at the rotation of the X- and Y-motors by a photoelectric chopper, which consists of a lamp, a silicon photodiode and a hole-disc mounted on the shaft of each motor. As long as one of the motors is rotating, pulses are generated, which are amplified and rectified separately in each channel. The output current of the rectifiers bring a negative charge into a capacitor, which is also connected to a positive voltage via a large resistor. The voltage of the capacitor is monitored by a dc-amplifier, that turns on a relay, if the input voltage exceeds a few volts positive.

If not one of the motors rotate, there are no pulses generated, the capacitor is slowly charged positive and after about 20 seconds the alarm relay is excited and switches on an acoustic signal.

3.4.3.4 Power supply

All of the units are powered by a common supply. The various dc-voltages and the current for the filaments are derived from the ac line. The 400 c/s voltage, supplying the tank and servo systems, are supplied by a motorgenerator, later on by a transistorized inverter.

The voltages are stabilized as for as necessary.

3.4.3.5 Appendix to 3.4.3.1

Calculation of gain g, input impedance Z_{in} and source resistance R_{out} of the impedance transformer

V_1 is assumed ideal with infinite grid impedance. The various grid impedances, which would cause grid currents in the real tube, are expressed by an external impedance connected between grid and cathode. This is possible as

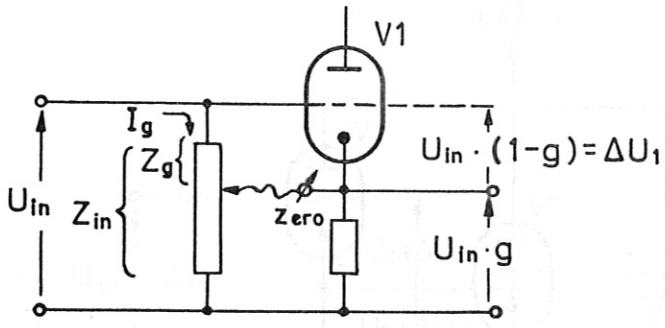

P 093

long as the voltages at the tube are kept constant. We further assume the grid dc-bias to be zero.

Then we see in P 093 that Z_{in} is increased by a cathode-follower:

$$\frac{Z_{in}}{Z_g} = \frac{U_{in}}{U_{in} - U_{in} \cdot g} = \frac{U_{in}}{U_{in}\,(1-g)} \qquad (1)$$

$g < 1$ is the real amplification

The expression $U_{in}\,(1-g)$, representing the "loss of signal voltage", is a significant term, which allows to calculate the characteristic figures of the circuit in simple and in structive manner.

For $Z_{in} \rightarrow \infty$ we must realize $g \rightarrow 1$. That means:

$$U_{in}(1-g) = \Delta U_1 \rightarrow 0 \qquad (1a)$$

ΔU_1 is the offset of the grid-cathode-voltage from an arbitrary dc-bias caused by applying an input signal U_{in} to the grid.

In a triode is the relationship between:

plate voltage U_p

plate current J_p

and grid voltage U_g :

$$\Delta U_g = \frac{\Delta Jp}{S} - \frac{\Delta Up}{\mu} \qquad (2)$$

S = transconductance

μ = amplificationfactor

For $\Delta U_1 = 0$ we have to keep constant J_{p1}; $(\Delta J_{p1} = 0)$ and U_{p1}; $(\Delta U_{p1} = 0)$, with other words: the operating point of V_1 may not change when the input signal U_{in} is applied. Grid current $J_{g1} \ll J_{p1}$.

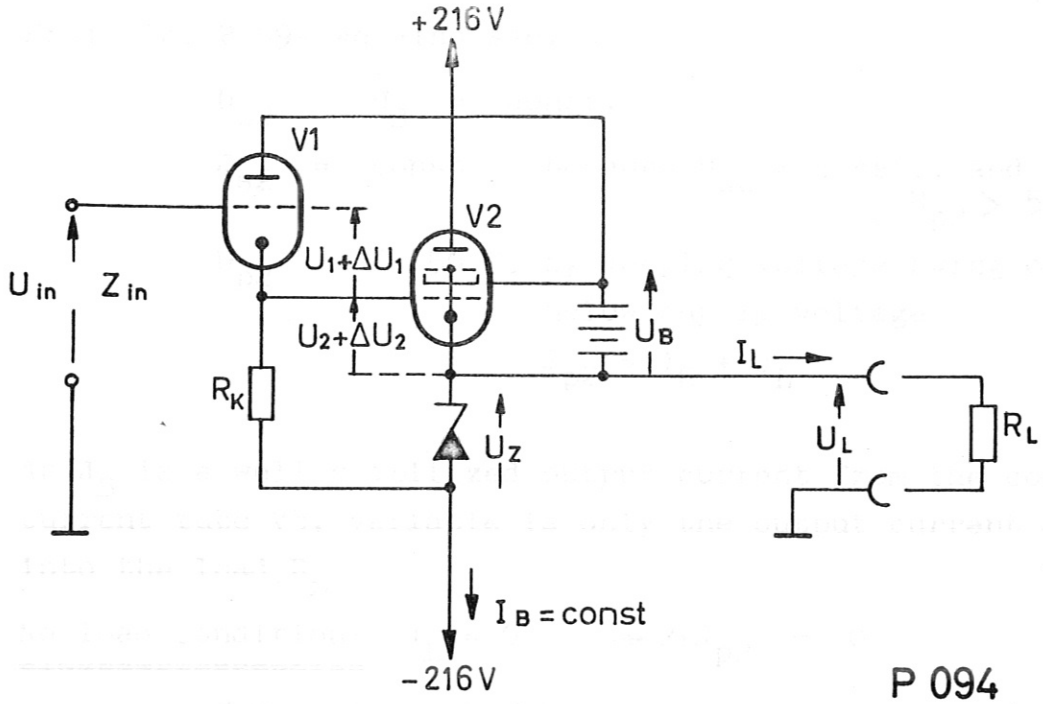

From P 094 we can see

$$J_{p1} + \Delta J_{p1} = \frac{U_Z + U_2 + \Delta U_2}{R_k} \qquad (3)$$

where:

U_Z = const. (Zenervoltage)

U_2 = dc-grid bias of V_2

U_B = const. supply voltage (floating)

$$U_{p1} + \Delta U_{p1} = U_B - U_2 - \Delta U_2 \qquad (4)$$

The single variable $\Delta U_2 \rightarrow 0$ if analog to V_1 those currents and voltages, which effect bias U_2 are kept constant. In a pentode there are

screen voltage	U_s
screen current	J_s
plate current	J_p

plate voltage has poor effect on the grid bias, as long the ratio J_p/J_s is not effected by too low plate voltage.

From fig. P 094 we also see:

$U_{s2} = U_B = \text{const.}$

$J_{s2} = \text{const.}$, because $U_{s2} = \text{const.}$, and $U_{p2} > 50$ V

$U_{p2} > 50$ V, by keeping voltage swing of U_{in} below supply voltage

$$J_{p2} = J_B + J_L \qquad (5)$$

As J_B is a well stabilized output current from the constant current tube V3, variable is only the output current J_L into the load R_L

No load condition: $J_L = 0 \rightarrow \Delta J_{p2} = 0$

$\Delta U_2 = 0 \rightarrow \Delta U_1 = 0$

$g_2 \sim 1 \qquad g_1 \sim 1 \qquad Z_{in} \rightarrow \infty$

we measured in the realized impedance transformers:

$g = g_1 \cdot g_2 = 0.9924$

$Z_{in} > 5 \cdot 10^{10} \Omega$.

this limited specification may be caused by the residual influence of the plate voltage swing at V_2 and the internal resistance of the Zenerdiode U_Z.

Load condition: $J_L \neq 0$

$$J_{p2} = J_B + J_L \qquad (5)$$

$$\Delta J_{p2} = J_L = \frac{U_L}{R_L} = \frac{U_{in}}{R_L} \; ; \; R_L = \text{load}$$

$U_L \sim U_{in}$ as long as $g \sim 1$ and if we neglect dc bias U_1 and U_2.

This is possible, because these constants do not affect the signal voltages. In dc amplifiers the dc podest $U_1 + U_2$ at the output can be eliminated by a potentiometer shunted to the zenerdiode, whose slider is connected to the output.

ΔJ_{p2} affects U_2 : $\quad S = \frac{\Delta J_{plate}}{\Delta U_{grid}}$

transconductance S of a pentode is fairly independant of plate voltage.

Signal loss in V_2:

$$\Delta U_2 = \frac{\Delta J_{p2}}{S_2} = \frac{U_{in}}{R_L \cdot S_2} \qquad (6)$$

Influence to V_1:

$$\Delta U_1 = \frac{\Delta J_{p1}}{S_1} - \frac{\Delta U_{p1}}{\mu_1} \qquad (2)$$

$$\Delta J_{p1} = \frac{\Delta U_2}{R_k} = \frac{U_{in}}{R_L \cdot R_k \cdot S_2} \quad \text{(from 3 ; 6)} \qquad (7)$$

$$\Delta U_{p1} = -\Delta U_2 = -\frac{U_{in}}{R_L \cdot S_2} \quad \text{(from 4 ; 6)} \qquad (8)$$

Signal loss in V_1:

$$\Delta U_1 = \frac{U_{in}}{R_L \cdot S_2} \left(\frac{1}{s_1 \cdot R_k} + \frac{1}{\mu_1} \right) \text{(from 2 ; 7; 8)} \qquad (9)$$

Total signal loss $\Delta U = \Delta U_1 + \Delta U_2$:

$$\boxed{\Delta U = \frac{U_{in}}{R_L \cdot S_2} \left(\frac{1}{R_k \cdot S_1} + \frac{1}{\mu_1} + 1 \right)} \qquad (10)$$

(from 6 ; 9)

now we can express:

Total gain g $\qquad g = 1 - \frac{\Delta U}{U_{in}}$ (from 1a)

$$\boxed{g = 1 - \frac{1}{R_L \cdot S_2} \left(1 + \frac{1}{R_k \cdot S_1} + \frac{1}{\mu_1} \right)} \qquad (11)$$

(from 10)

Increase of Z_{in} at given Z_g of the real tube:

$$\frac{Z_{in}}{Z_g} = \frac{U_{in}}{\Delta U_1} \qquad \text{(from 1 ; 1a)}$$

$$\boxed{\frac{Z_{in}}{Z_g} = \frac{R_L \cdot S_2}{\frac{1}{S_1 \cdot R_k} + 1/\mu_1}} \qquad (12)$$

Source resistance at the output:

$$R_{out} = \frac{\Delta U}{D_L} = \frac{\Delta U \cdot R_L}{U_{in}} \qquad (13)$$

$$\boxed{R_{out} = \frac{1}{S_2}\left(1 + \frac{1}{R_k \cdot S_1} + \frac{1}{\mu_1}\right)} \qquad (14)$$

(from 10; 13)

As example, we calculate these 3 important figures g, Z_{in}, R_{out}.

Dimensions given:

R_k = 33 kΩ
R_L = 7,2 kΩ
S_1 = 2 mA/V +)
S_2 = 4 mA/V +)
μ_1 = 35

$$g = 1 - \frac{1}{7{,}2 \times 4}\quad 1 + \frac{1}{33 \times 2} + \frac{1}{35}$$

$$= 1 - 0{,}0348\ (1 + 0{,}015 + 0{,}029)$$

$$1.044$$

$g = 0{,}9637$ calculated

$g = 0{,}958$ measured

+)
the transconductance is lowered by the reduced J_{p1} or U_{p2}

$$\frac{Z_{in}}{Z_g} = \frac{7.2 \times 4}{0.044} = 650$$

$$Z_{in} = 650\, Z_g \quad \text{calculated (not measured)}$$

$$R_{out} = \frac{10^3}{4} \quad (1.044) = 260\ \Omega$$

3. 5 Tests on components and on detail models of individual parts and critical sections

In order to investigate the behaviour of components under severe electrical or mechanical stress, detail models in a scale of 1 : 1 are prepared and subjected to life tests exerting the original stress. These tests determine the materials and geometrical dimensions used. Statements on the lifetime of the components are also based on these fatigue tests. The geometrical shape of collector zones under severe electrical stress was checked in detail models with low-current input.

3. 5.1 Current tests

3. 5.1.1 Contacts for the 1.5/2.5 MJ capacitor bank

The appropriate contact material and geometrical form of a combination of contacts was determined in preliminary tests on contactors 1 cm wide. Copper was chosen as contact material and the contacts were arranged with a plane surface against a cylindrical surface.
In order to subject the choice of contactors to life tests exerting the original stress among other reasons, a detail model of 1/18 of the original collector configuration was constructed.

3. 5.1.2 144 kJ test bank

The 1/18 section of the collector serves another purpose. It is supplied by a 144 kJ capacitor bank specially built for testing purposes and is used for testing improved versions of contacts new designs of load coils and various other components under stress due to high currents. At a charging voltage of 40 kV currents of the order of 1 MA can be attained in this device.

3. 5.1.3 Plug contacts

Because of the small cable graduation at the collector connection (50 mm horizontal, 60 mm vertical) of the

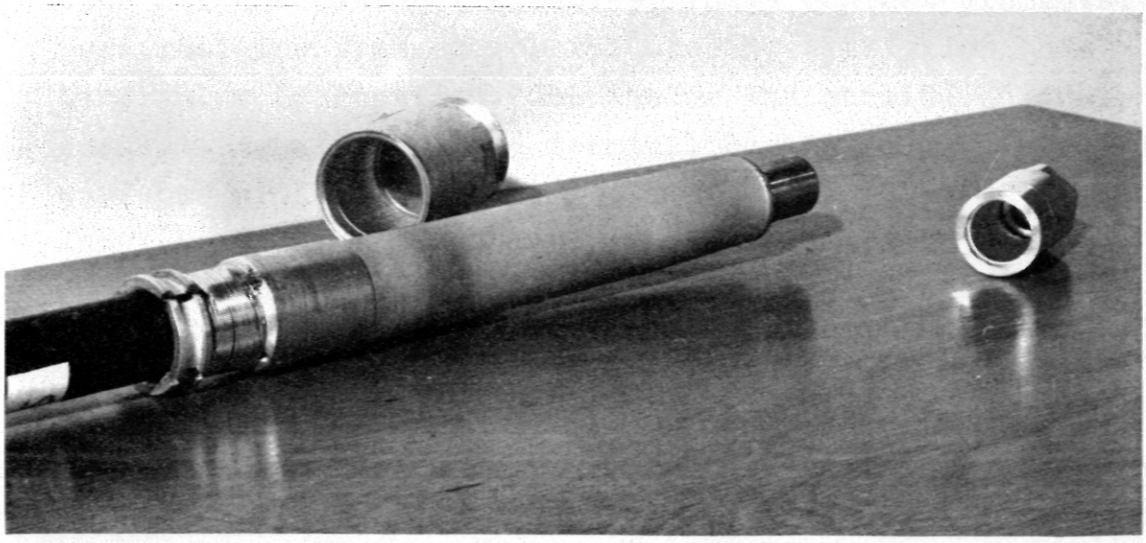

P 037 500 kJ - Theta-Pinch

Pulse cable terminal and contact element

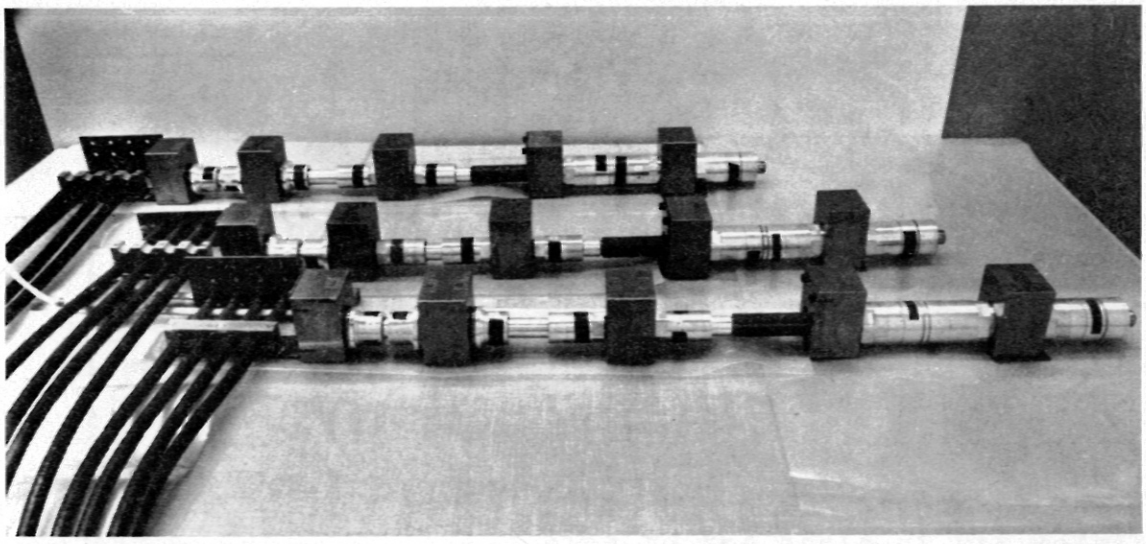

P 038 500 kJ - Theta-Pinch

Test rig for pulse cable contact elements

500 kJ bank, plug-in contacts were chosen for the first time for contacting the cables. These contact elements, were resigned from commercial ones specially for this particular application. The inside and outside conductor connections at the cable terminal consist of cylindrical surfaces with the following dimensions:
Inner conductor: length = 50 mm, diam. = 22 mm
Outer conductor: length = 42 mm, diam. = 38 mm

The contact surfaces of the socket is formed by springs arranged axially on a cylindrical surface. The current passes from the plug part of the cable via these springs to the solid part of the socket (Fig. P 037). No information was available on the behaviour of such contacts in pulsed operation. An experimental device was therefore set up in which the contacts are rested with twice the original stress (30 kA, 100 kHz, 70 % reversal) (Fig. P 038). The sample sockets withstood 20,000 discharges without visible destruction.

3 .5.1.4 Low-current models

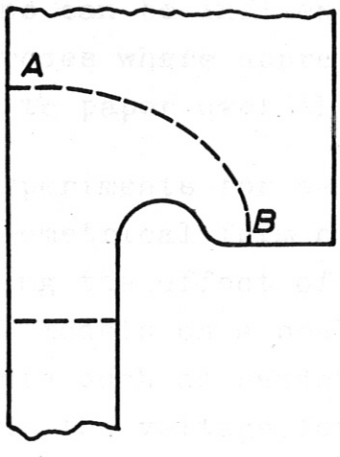

Fig. P 091

In collector configurations transitions of the type shown alongside occur. With respect to the stress the current density distribution at the regions of transition is of interest. The current density distribution was measured in an enlarged detail model by means of the coil probes. (measured voltage proportional to the current density at conductor surface). The input voltage frequency was chosen according to the scale of the model. The boundary condition, i.e. the position of the feeding points along the line AB was determined

from a flow diagram of the complete configuration. The detail was chosen such that AB is roughly equivalent to an equipotential line.

3. 5.2 Voltage tests

The insulation material of plate-type collector configurations commonly consists of several layers of foil. The regions at which one insulating layer is succeeded by a second layer of the same or of a different kind, e.g. the transition between the precollector and main collector, are always critical. At these points the two insulating layers are overlapped or inserted into one another so that the leakage path is large enough to prevent leakage breakdown, the overlap length being kept as small as possible (with regard to the inductance of the configuration).

The overlap length required depends, on the one hand, on the type and composition of the surface of the insulating material and, on the other, the elecetrode shape plays an important part. The conducting layers in collectors are most often made of sheet copper (e.g. 2 mm thick). At the edges and turns of the sheeting there occur corona discharges which lead to breakdown on the foil insulation. The potential distribution at the critical transition regions can be influenced by incorporating voltage grading electrodes where appropriate or sticking semiconducting graphite paper over the conductors.

The experiments for selecting the insulating material and the geometrical form of transitions and corners and for checking the effect of potential control are conducted on detail models on a scale of 1 : 1 at the oroginal frequency. Elements such as sandwich conductors and cables which determine the voltage form are incorporated in the original in the experimental circuitry.

The tests are conducted at 1.2 times the nominal voltage and are normally continued for the guaranteed lifetime

(20.000 discharges). The rapid discharge sequence in the model experiment represents a further tightening of the testing conditions.

3. 6 Electrical analogon to the collector motion

Because of the high discharge currents involved collector configurations of high-energy capacitor banks are subject to very severe pulse stress. In the main collector for the Isar I experiment, for instance, the peak force is in the order of 10^4 t. In this connection the motion permitted to the conducting layers is of the order of only approx. 50 /u. The problem can be solved in three ways:

1) The two halves of the collector are braced against one another.
2) Starting from the line of symmetry the collector is arranged as follows: conducting layer - steel pressure plate - lead or concrete mass (designed according to the pressure distribution determined from the field of flow). In the top half of the collector these masses rest free under their force of gravity, while in the bottom half they are pressed upwards via springs by twice their own wieght. The system is thus symmetrical to the horizontal line of symmetry.
3) It is also possible to combine solutions 1) and 2), putting a stronger emphasis on one or the other.

In practice it has been shown that calculating the motion process of the individual masses is a complicated and very cumbersome business. It was therefore attempted to solve the problem using an electrical analogon.

The connections relating the present mechanical spring-mass system and the electrical analogon are as follows:
A mass is replaced by an inductance, a spring by a capacitor, and friction by resistance. A series connection in the mechanical system is altered to a parallel electrical circuit in which forces are represented by voltages and

displacement by charge:

Force	-	Voltage
Mass	-	Inductance
Spring	-	Capacitor
Friction	-	Resistance
Displacement	-	Charge
Velocity	-	Current
Acceleration	-	Current derivation

3. 6.1 Model of the collector of the 1.5/2.6 MJ capacitor bank Isar I

Whereas solution 1) with lead plates as weights was used in the main collector, a combined solution (concrete weights and support structure) was prefered in the collector extension.

Fig. P 092 below shows the equivalent mechanical diagram and the electrical analogon of the configuration for the collector extension.

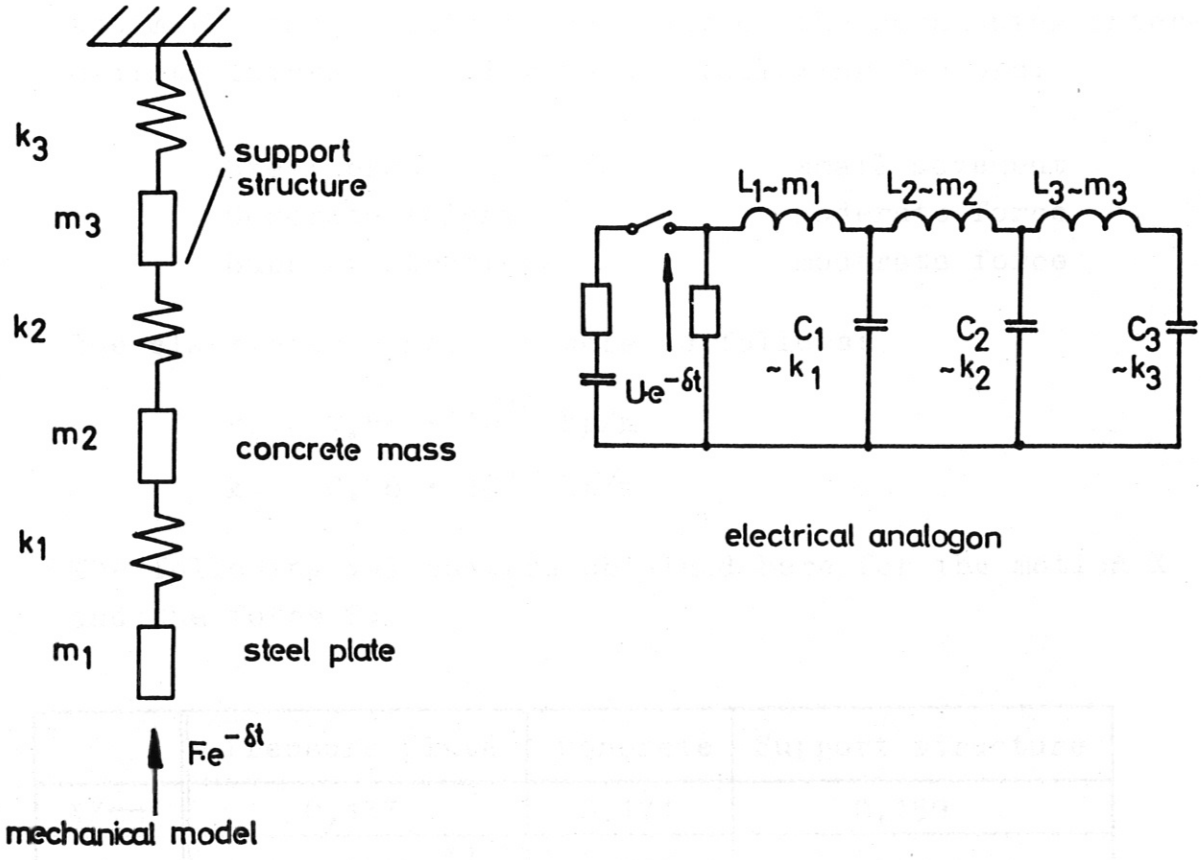

P092 Mechanical model and electrical analogon of a collector system

To allow for small motions and forces the masses have to be chosen as large as possible.
The design has the following values:

m_1 = steel pressure plate = 1.5 t
m_2 = concrete mass = 2.4 t
m_3 = support structure = 2.5 t

The elasticity constant of the bracing is:

$$k_3 = 0{,}39 \cdot 10^{10} \ \frac{kp}{m}$$

3. 6.1.1 Measurements

The mechanical mass-spring system is acted on by a force

$$F \cdot e^{-\delta \cdot t}$$

where F = 9500 t

$$\delta = 2.6 \cdot 10^4 \ s^{-1}$$

The electrical analogue measurements were used to determine optimally the elasticity constant of the cushioning intermediate layers according to the following factors:

Steel pressure plate	small movement
Concrete weight	moderate force
Support structure	moderate force

The elasticity constants were as follows:

$k_1 = 1{,}56 \cdot 10^{10}$ kp/m
$k_2 = 0{,}78 \cdot 10^{10}$ kp/m

The following values were obtained here for the motion X and the force F:

	Pressure plate	Concrete	Support structure
X/mm	0,133	0,171	0,159
F/t	1500 (9500)*)	1700	1000

*) = first, very short peak .

This work was performed under the terms of the agreement on association between the Institut für Plasmaphysik and EURATOM